M. Kageyama · F. D'Andrea · G. Ramstein · P. J. Valdes R. Vautard

Weather regimes in past climate atmospheric general circulation model simulations

Received: 17 November 1999 / Accepted: 2 May 1999

Abstract We investigate the climates of the presentday, Inception of the Last Glaciation (115000 y ago) and Last Glacial Maximum (21 000 y ago) in the extratropical north Atlantic and Europe, as simulated by the Laboratoire de Météorologie Dynamique Atmospheric General Circulation Model. We use these simulations to investigate the low-frequency variability of the model in different climates. The aim is to evaluate whether changes in the intraseasonal variability, which we characterize using weather regimes, can help describe the impact of different boundary conditions on climate and give a better understanding of climate change processes. Weather regimes are defined as the most recurrent patterns in the 500 hPa geopotential height, using a clustering algorithm method. The regimes found in the climate simulations of the presentday and inception of the last glaciation are similar in their number and their structure. It is the regimes' populations which are found to be different for these climates, with an increase of the model's blocked regime and a decrease in the zonal regime at the inception of the last glaciation. This description reinforces the conclusions from a study of the differences between the climatological averages of the different runs and confirms the northeastward shift to the tail of the Atlantic

M. Kageyama¹ (☒) · G. Ramstein
Laboratoire des Sciences du Climat et de l'Environnement,
CE Saclay, L'Orme des Merisiers, Bâtiment 709,
91191 Gif-sur-Yvette, France
E-mail: masa@lsce.saclay.cea.fr

Also at:

¹ Department of Meterology, University of Reading, United-Kingdom

P. J. Valdes Department of Meteorology, University of Reading, United-Kingdom

F. D'Andrea · R. Vautard Laboratoire de Météorologie Dynamique, Ecole Normale Supérieure, Paris, France storm-track, which would favour more precipitation over the site of growth of the Fennoscandian ice-sheet. On the other hand, the Last Glacial Maximum results over this sector are not found to be classifiable, showing that the change in boundary conditions can be responsible for severe changes in the weather regime and low-frequency dynamics. The LGM Atlantic low-frequency variability appears to be dominated by a large-scale retrogressing wave with a period 40 to 50 days. In addition weather regimes are found in a sector located further eastward over the east Atlantic and European continent and are proved to be linked to this low-frequency oscillation.

1 Introduction

1.1 Objectives

For the present climate in the Northern Hemisphere extra-tropics, there is now much evidence, using different methods, that the intraseasonal variability of the atmospheric circulation can be described by transitions between a small number of states, or weather regimes. For example, the European winter weather can often be reminiscent of a zonal or a blocked regime (see Dole and Gordon 1983). The zonal regime is characterized by a relatively warm, wet and anomalously perturbed weather over most of Europe, while anticyclonic, dry and cold conditions prevail during blocked periods, with perturbations being directed to the north and the south of the anticyclone (see Nakamura and Wallace 1990 for a composite synoptic study). Weather regimes are thus strongly linked to local weather, characterized by e.g. surface temperature and precipitation.

The present work studies weather regimes in atmospheric general circulation model (AGCM) simulations of the climates of the present (CTRL), Last Glacial Maximum (LGM, 21 000 y ago) and Inception of the Last Glaciation (ILG, 115 000 y ago). While the LGM

climate is an extreme, much colder than the present climate in the extra-tropical latitudes, the ILG climate seems quite similar to ours, but eventually led to the progressive build-up of the ice-sheets over northern North America and Scandinavia, that would culminate at the LGM. Hence the study of palaeoclimate simulations involves analyzing large (e.g. the LGM case) as well as more subtle (e.g. the ILG case) climate changes.

Palaeoclimate AGCM simulations are traditionally analyzed in terms of climatological averages, but this approach may not be ideal. Indeed such averages do not account for the variability of the atmospheric circulation and small changes in the climatological means may hide large ones, e.g. in extreme weather events, that would nearly cancel out when averaged. For recent and future climate changes, Ghil and Childress (1987) and Palmer (1993, 1998) have suggested a method which could be potentially both more useful and insightful to analyze climate changes. According to their ideas, climate change can be seen as a modification in the weather regime populations, which are linked to the probability distribution of local weather events. Our main objective is to determine whether such an approach can be applied to describe post climate changes in a sector such as the North Atlantic and if this new and different analysis of past climate change helps improve our understanding of climate dynamics. We cannot directly prove or disprove the model changes, as the palaeorecord cannot tell us anything about the lowfrequency variability, although some indicators may be sensitive to different weather regimes.

A first step is to estabish if the regimes of a past climate are the same as for the control. If they are the same, the changes in the population of the regimes can be evaluated. A subsidiary problem is to examine to which extent the regimes of the control experiment can be used to study past climate changes. This work addresses these questions thanks to long (45 y) AGCM simulations of the climates of the present-day, the Inception of the Last Galciation and the Last Glacial Maximum. A duration of 45 y has been chosen for our runs because it compares well with the observational data currently available, for which most algorithms have been developed.

The LGM simulation is the standard PMIP (Palaeoclimate Modelling Intercomparison Project, Joussaume and Taylor 1995) run performed at Laboratoire des Sciences du Climat et de l'Environnement, lengthened to 45 y. For the Inception of the Last Glaciation, we performed several simulations, to evaluate the sensitivity of the climate of this period to changes not only in the insolation, which is thought to be primarily responsible for the timing of the glacial-interglacial cycles, but also in the sea-surface temperatures and vegetation cover. Those last factors have indeed recently been proved to have been quite different in the northern high latitudes at the Inception of the Last Glaciation, as is discussed in more detail in Sect. 2.2.1.

We focus on the winter climate over the North Atlantic and Europe, and the characteristics of each regime in terms of surface temperature, storminess and precipitation. The reason for this is threefold. First, we want to study the precipitation changes in the ILG and LGM experiments because they are important in the ice-sheet mass budget. The main source of precipitation in this area being extra-tropical weather systems, it appears natural to study the winter climate, in which they are most active. Second, most of the studies of weather regimes have been carried out for the winter season, for which the variability of the atmosphere in this region is largest. Analyzing the winter climate therefore helps compare our results with previous studies. Third, there has been much concern recently about the possible impact of global climate change on extreme events and storminess in mid-latitude regions such as Europe (see Schmith et al. 1998 for an analysis of the storminess over the last 120 years, Hall et al. 1994 and Carnell et al. 1996 for a study of storminess in simulations with doubled CO₂ concentration). The question is open as to whether there could be a change from the present weather regime populations. Our study addresses this problem in similar or very different past climates.

We give a brief review on the weather regimes' relationship to local weather in Sect. 1.2, and on the studies on changes in weather regime population during recent climate anomalies in Sect. 1.3. In Sect. 2, the AGCM and the experiments are described. Section 3 is dedicated to the weather regimes in the present day climate simulation, while Sect. 4 deals with weather regimes in the past climate experiments. Conclusions and perspectives are given in Sect. 5.

1.2 Weather regimes and local weather

The concept of weather regimes originates from studies on atmospheric blocking (Rex 1950a, b) whose peculiar recurrence and persistence was difficult to explain theoretically. Later Charney and De Vore (1979) found multiple stationary solutions in the governing equations of a simple model and associated the phenomenon of blocking with one of these equilibria. This and subsequent works led to the concept of weather regimes, also applied later to observational data by Mo and Ghil (1988), and since by many other authors. As reviewed by Michelangeli et al. (1995) (hereafter MVL), there are several approaches to define weather regimes, based on their different properties: persistence, recurrence, and quasi-stationarity. In fact, very few authors have really defined weather regimes from one of these properties and studied local weather characteristics such as temperature or precipitation typical of these regimes. However, many more have investigated the simultaneous low-frequency variability of these variables and give an account of the correspondence between anomalies in the mid-tropospheric circulation and local weather.

Among the authors who defined weather regimes from one of the three properties mentioned and studied the associated characteristics in other variables, Dole (1986) finds a marked change in the location of the storm-tracks (here storm-track defines regions of large variability on synoptical scales, from 2 to 6 days, due to high-frequency transients) according to the regime: over the North Atlantic, during persistent positive anomalies in the 500 hPa geopotential height (hereafter z500), the tail (i.e. eastern end) of the storm-track shows a significant displacement to the north, whereas during persistent negative anomalies the storm-track is very zonal. Furthermore, Ayrault et al. (1995), defining their weather regimes as the most recurrent atmospheric circulation patterns, show that perturbations growing on time scales smaller than two days develop in different areas according to the regime. It is therefore possible to link large-scale weather regimes to mesoscale and surface features.

Lau (1988) analyzed the month-to-month variability of the northern extratropical mean flow patterns on the one hand, and of the high-frequency transients on the other. He finds a strong correspondence between the low-frequency variations of these two types of quantities. Fraedrich et al. (1993) use this idea that weather regimes should be retrievable from simultaneous variations of several quantities and define their weather regimes by performing an EOF analysis of a single vector containing European precipitation, temperature and mean sea-level pressure data. Their first EOF corresponds to the alternative between the blocked and the zonal regimes and their typical surface characteristics, mentioned earlier, showing that regimes can be consistently defined using one or several variables.

Some general circulation models have been proved to be able to reproduce the pattern of the low-frequency variability of the atmosphere quite satisfactorily (Ponater et al. 1994; Michelangeli 1996). However, Tibaldi et al. (1997), who study the blocking climatology in four integrations of the same model as Ponaer et al. (1994), report that all the versions of the model tend to underestimate the blocking occurrence, even though its performance improves with resolution and better physical parametrizations. This difficulty in representing blocking correctly is found in many models, as shown in the AMIP (Atmospheric Modelling Intercomparision Project) studies of D'Andrea et al. (1996, 1998). We return to the limitations of the AGCM used in the present work in Sects. 2.1 and 3.2.

1.3 Climate anomalies and weather regimes

The idea that climate change can be characterized by a change in weather regime populations has already been followed by a number of authors in their analysis of the interannual variability of present climate. In the early 1960s Dzerdzeevskii (1962) analyzed the fluctuations of the climate in the first half of the century by examining the changes in the populations of 'zonal' and 'meridional' regimes. More recently, Ghil and Childress (1987) have outlined the advantages of using the concept of weather regimes to study the atmospheric response to sea surface temperature (SST) linked to El-Ninõ-Southern-Oscillation (ENSO). Fraedrich et al. (1992) show that Dzerdzeevskii's (1962) 'zonal' regime of the northern extra-tropical circulation is enhanced (reduced) after an El-Niño (La Niña) year; the Pacific storm-track's tail in particular shifts southward (northward) after warm (cold) events. In other studies on the influence of ENSO in the European climate, Fraedrich (1990, 1994) reports a cyclonic (anticyclonic) regime during a warm (cold) event.

Some other works have used, as is done here, cluster analysis to define their regimes as the most recurrent atmospheric circulation patterns: Molteni et al. (1993) use clusters obtained by Molteni et al. (1990) for the present-day climate to analyze climate runs forced by SSTs characteristic of a La-Niña year, with a cold equatorial eastern Pacific. They find that such an anomaly favours one of the regimes, which corresponds well to the observations for the La-Niña year they study. Blender et al (1997) analyze the North Atlantic cyclone tracks and find a stationary, a northeastward and a zonal group of cyclone trajectories. They find that the moisture transport is mainly northeastward (zonal) during winters of high (low) North Atlantic Oscillation (NAO) index, and that the main direction of these fluxes where explained by the dominant cyclonetrack regime.

Robertson et al. (1999) extract the weather regimes from a long ECHAM simulation of the present climate, and then study how the populations of these regimes change in a 10-y long simulation forced by SSTs with a warm anomaly in the North Atlantic. They find that this is a more convincing (i.e. statistically significant) way to describe the climate change than conventional climatological field differences. In their case, they report a response typical of the positive (zonal) phase of the NAO. They explain that the response as described by weather regime population changes is clearer because fewer variables are used to describe a climate simulation.

Nevertheless, the assumption that regimes are the same under different boundary forcings is not a trivial one. Ferranti et al. (1994b), in another study on the influence of localized SST anomalies in the Northern Hemisphere circulation, suggest that perturbed SSTs can not only decrease or increase the population of a regime, but also change the degree of separation between the regimes, or even the number of regimes. In simulations of palaeoclimates, for which the changes in boundary conditions can be much larger than the ones

imposed in the studies mentioned, this could well happen. This is one of the main questions we want to address here.

2 Model and simulations

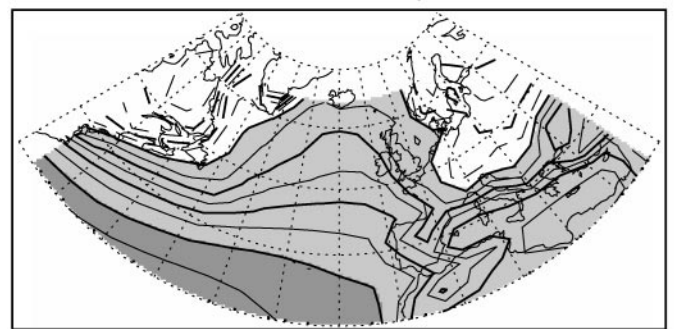
2.1 Present climate (CTRL) simulation

The atmospheric general circulation model used in the present study is the model from the Laboratoire de Météorologie Dynamique (LMD), in its version 5.3. This model, first described by Sadourny and Laval (1984), is a grid-point model using a grid which is regular in longitude and sine of the latitude, all gridboxes therefore having the same area. The version used here is the same as the one described and used in Harzallah and Sadourny (1995) and has the same resolution (64 points in longitude, 50 in sine of the latitude and 11 irregularly spaced vertical levels). Its performance is typical of a relatively low-resolution model, with in particular, quite short and weak storm-tracks as pointed out by Harzallah and Sadourny (1995) and Kageyama et al. (1999). This is explained by the fact that baroclinic eddies are not resolved with a very high accuracy compared to higher resolution models (Seluchi et al. 1998; Kageyama et al. 1999).

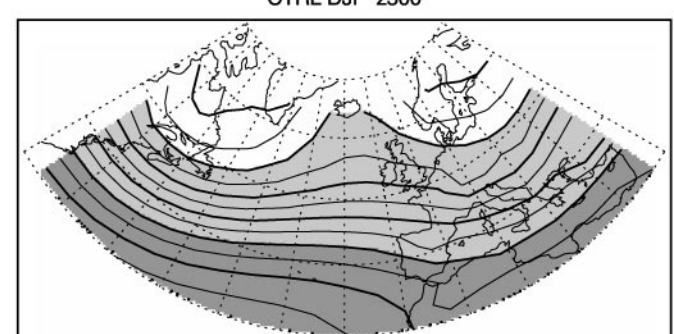
A particular feature of the model is its detailed representation of the land-surface and of the land-surface-atmosphere interface, thanks to the SECHIBA scheme (Ducoudré et al. 1993). This allows for an asynchronous coupling with a biome model, after which a vegetation in equilibrium with the climate simulated by the AGCM is obtained (for details on the method used, see DeNoblet et al. 1996 and Texier et al. 1997). Vegetation changes have been suggested as an important mechanism for the inception of the last glaciation (see Sect. 2.2.1) and some of the simulations of the ILG climate studied here include these changes in vegetation cover. The CTRL and LGM simulations have been run with the standard eight biome AGCM, while all the ILG simulations have been run using the version of the AGCM in which 17 biomes are represented, which allows for the coupling with the biome model. The control simulation using the 17 biome version of the AGCM (CTRLV) is very similar to the CTRL results presented in Fig. 1 and is not described here.

Figure 1 gives a summary of the present winter (December-January–February) climate as simulated by the model in the sector (80 °W-40 °E, 30-70 °N) studied here. For the 45-y-long simulation, SSTs have been prescribed to the seasonally varying climatological average of the AMIP SSTs, complying with the directives of the Palaeoclimate Modelling Intercomparison Project (PMIP, Joussaume and Taylor 1995). The surface air temperature over the North Atlantic (top left Fig. 1) reflects the SST pattern, with a strong meridional gradient in the west Atlantic which weakens in the eastern part of the basin and tightens again above the northern Mediterranean coast. The tightest meridional temperature gradients are in fact associated with the contrast between the cold continents and the warmer oceans, over the American east coast and the Mediterranean north coast. This pattern in surface temperature is retained in the z500 mean field (top right Fig. 1), which shows a strong jet-stream over the west Atlantic which decreases eastward, and strengthens again over southern Europe. The flow is therefore most baroclinic over the west Atlantic and southern Europe, and the storm-tracks' maxima are located over and downstream of these

CTRL DJF surface air temperature



CTRL DJF z500



CTRL DJF z500 std deviation

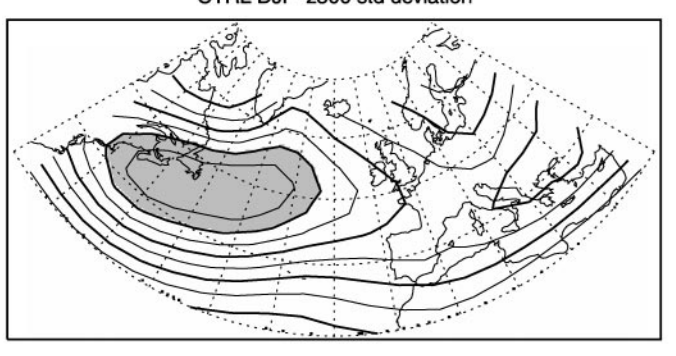
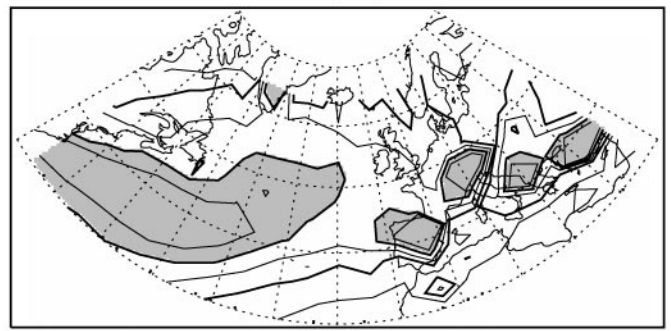


Fig. 1 DJF climatological averages for the CTRL run. *Top-left*: surface air temperature, contours every $2.5\,^{\circ}\mathrm{C}$ from -25 to $+25\,^{\circ}\mathrm{C}$, *light shading* from 0 to $15\,^{\circ}\mathrm{C}$, *dark shading* above $15\,^{\circ}\mathrm{C}$; *top-right*: $500\,\mathrm{hPa}$ geopotential height, contours every $50\,\mathrm{m}$ from 4800 to $5800\,\mathrm{m}$, *light shading* from 5300 to $5600\,\mathrm{m}$, *dark shading* above $5600\,\mathrm{m}$;

CTRL DJF precipitation



bottom-left: 500 hPa geopotential height high-pass filtered standard deviation, contours every 5 m from 0 to 100 m, shading above 50 m; bottom-right: precipitation, contours every 1 mm/day from 0 to 5 mm/day shading above 4 mm/day

regions (bottom left Fig. 1). Here, we define the storm-tracks using a high-pass filtered z500 standard deviation. The filter used is the Lorenz 'poor man' filter detailed in Hoskins et al. (1989), which is aimed at retaining synoptic variability, in a band of two to six days. The storm-tracks is shorter and weaker than observed (Kageyama et al. 1999), which is frequently so for models of this resolution, and this can explain the slightly weaker precipitation over the Atlantic basin (bottom right Fig. 1). The high precipitation values around the northern Mediterranean coast are the result of a few elevated gridpoints along with the secondary maximum in storminess mentioned earlier. The model therefore simulates the main features of the winter climate over the North Atlantic/European sector satisfactorily enough to be worthwhile to study the low-frequency (intraseasonal) variability of these features.

2.2 Past climate simulations: methodology

The LMD model has also been used extensively at Laboratoire des Sciences du Climat et de l'Environnement for palaeoclimate simulations. The LGM simulation with this version has been examined by Masson et al. (1998) and Ramstein et al. (1997) and some of the ILG simulations have been studied by DeNoblet et al. (1996). All the experiments here use prescribed, seasonally varying, climatological SSTs, which are deduced from palaeoindicators for the palaeoclimate runs. Indeed, it is difficult to devise prescribed SST palaeoclimate experiments with SSTs that include interannual variations. This constitutes one of the limitations of our study, since the lowfrequency atmospheric variability induced by SST interannual variability is not negligible (Harzallah and Sadourny 1995). However, the time scale of weather regimes is more in the intraseasonal range (typically more than a week and less than a month) than in the interannual one and they are usually considered to be the result of the internal variability of the atmosphere, especially in the northern Atlantic sector considered here (MVL). Indeed, Vautard and Legras (1988) show that in a two-layer channel model, different regimes can be sustained with only the influence of the transient eddies, and no orography or slow variations of the lower boundary condition. Furthermore, the fact that our weather regimes (Sect. 3) are not dissimilar to the observed ones justifies our approach a posteriori.

Other boundary conditions to the model include the insolation forcing, the CO₂ concentration and the land-surface conditions (vegetation and land-ice distribution). The characteristics of the simulations are summarized in Table 1 and detailed separately for the two periods in the following subsections.

2.2.1 Inception of the Last Glaciation (ILG) experiments

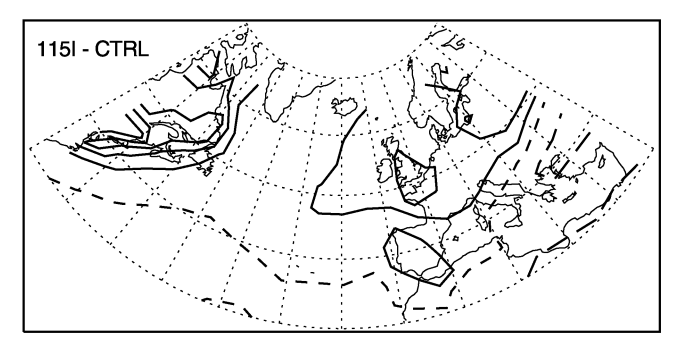
The Inception of the Last Glaciation has for long been considered as a test of the sensitivity of the atmospheric general circulation models (Royer et al. 1983). Indeed, it was first thought, according to the Milankovitch theory (Hays et al. 1976; Berger 1980) that the inception of the glaciation was primarily triggered by changes in the orbital forcing alone, which imply warmer winters and colder summers in the Northern Hemisphere. This forcing is not very large but the principle is that if the summers are cold enough, all the snow accumulated in winter cannot melt and starts accumulating; the albedo of the snow being very high, it tends to help maintain low temperatures, which in turn favours a longer duration of the snow cover and more snowfall rather than rainfall. The orbital forcing effect would therefore be amplified by this positive snow albedo feedback.

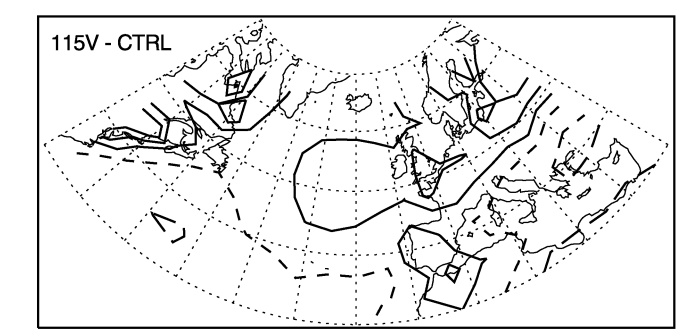
Until now, very few AGCMs have proved to be able to simulate the inception of the glaciation under the changes in orbital forcing alone (see Dong and Valdes 1995 for a review), and some modelling studies put forward the importance of interactions between the atmosphere and other components of the climate system, such as the vegetation (Gallimore and Kutzbach 1996; DeNoblet et al. 1996) or the ocean (Syktus et al. 1994, or Dong and Valdes 1995, using an AGCM coupled to a slab-ocean model; Ledley and Chu 1994, with a coupled energy balance climate-thermodynamic sea ice model, and many others). Among these hypotheses, some are supported by palaeodata evidence, in particular concerning the variations of the sea-surface temperature induced by thermohaline circulation changes during this period (Cortijo et al. 1994; Miller and de Vernal 1992; Ruddiman and McIntyre 1979). The decisive mechanisms as far as the growth of the ice-sheets is concerned is the summer temperature, which controls the melting of the snow. However, for ice-sheet growth to happen, they also need sufficient snow fall. The position of the storm-tracks, which constitute a main source for the precipitation in the areas where ice-sheets have developed, is closely examined in our simulations of the inception of the glaciation and the LGM climate. Ruddiman and McIntyre (1979) has suggested, from their data, that the storm-track position may have shifted so as to favour more snowfall over the Laurentide ice-sheet site. However, over the domain studied here, the largest changes are found for the east Atlantic and Europe and those will be our main focus.

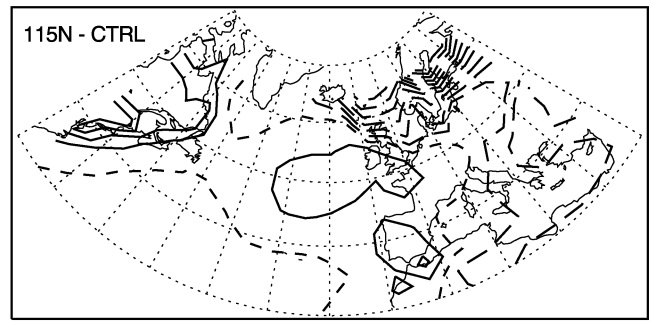
All the ILG experiments are summarized in Table 1 and will be described in greater detail in a subsequent study. The first simulation considered here, 115I, is 45 y long (all durations given exclude the first year of the simulations, during which the model equilibrates to its boundary conditions). It uses the same boundary conditions as the present-day climate run except for the CO₂ concentration which is set to a pre-industrial value (280 ppm instead of 345 in the control run) and the insolation which is set to values for 115000 y ago (Berger and Loutre, 1991). 15-year-long 115V uses the same boundary conditions but the model's vegetation is now in equilibrium with the climate, following the method described by DeNoblet et al. (1996, see their Fig. 4). They find that the summers are cold enough to induce a southward migration of the tundra-taiga limit, which helps maintain the snow throghout the summer: the taiga reduces the snow albedo feedback since the snow accumulates under

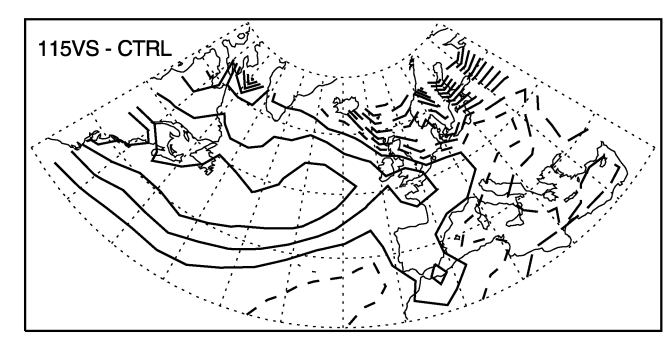
Table 1 Summary of the experiments studied in this paper. References for the CTRL and LGM simulations: Masson et al. (1998). Reference for experiments 115I and 115V: DeNoblet et al. (1996)

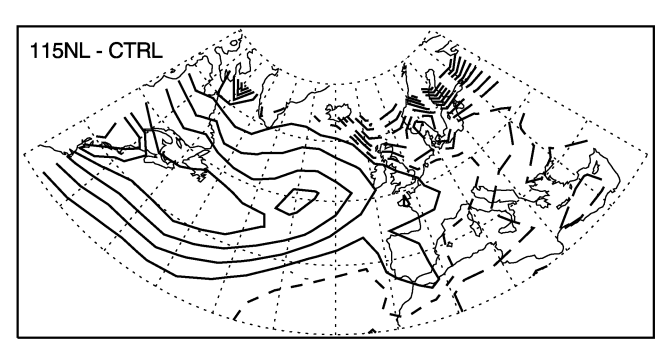
Simulation	Insolation	SSTs	Vegetation	Land-ice	Duration
CTRL	Present-day	AMIP climatology	Present	Present	45 y
115I	115 000 BP	Same as CTRL	Present	Present	45 y
115V	115 000 BP	Same as CTRL	In equilibrium with climate	Present	15 y
115N	115 000 BP	Colder Norwegian Sea	Present	Present	15 y
115NL	115 000 BP	Same as 115N with warmer Labrador Sea	Present	Present	15 y
115VS	115 000 BP	Same as 115NL	From 115V	Present	45 y
LGM	21 000 BP	CLIMAP (1981)	Present except where new land-ice	Peltier (1994)	45 y











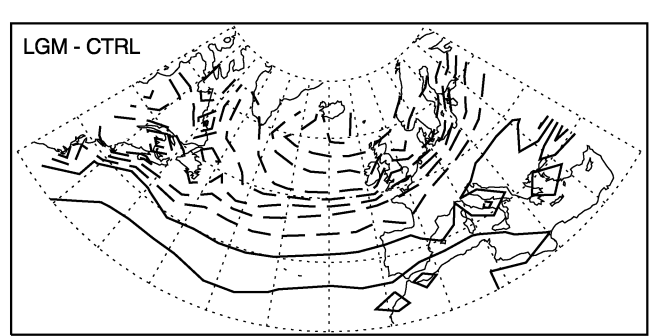


Fig. 2 Anomalies in surface air temperatures between past climate DJF climatological means and the control one. *Top-left*: 115I, *top-right*: 115V, *middle-left*: 115N, *middle-right*: 115VS, *bottom-left*: 115NL, *bottom-right*: LGM. Contours every 0.5 °C from -5

to $+5\,^{\circ}\text{C}$ with zero contour short-dashed and negative contours long-dashed, except for LGM, for which the contours are every 2.5 $\,^{\circ}\text{C}$ from -25 to $+25\,^{\circ}\text{C}$ and the -2.5 and $-5\,^{\circ}\text{C}$ contours are solid lines

the vegetation which keeps its albedo, whereas the tundra does not. The experiment 115N (15 y long) uses the same boundary conditions as 115I but with colder SSTs in the Norwegian Sea (data from CLIMAP 1984; Cortijo et al. 1994). For the winter season, in which we are interested here, this means that the sea-ice extent is larger in the Norwegian Sea, with a quasi-zonal southern limit just north of Iceland. The strong negative anomaly in surface air temperature over this region (Fig. 2) clearly shows the impact of this SST anomaly imposed to the model. 115NL (15 y long) uses the 115N boundary conditions with a warmer northwestern Atlantic Ocean and Laborador Sea (data from Miller and de Vernal 1992). The anomaly is mainly localized around Newfoundland, with a maximum amplitude of 3 °C. Again, its impact on the surface air temperatures of this region are clearly seen in Fig. 2. Note that this pattern, with a reversed polarity between the Laborador Sea and the west Atlantic off Newfoundland on the one hand, and the Greenland and Norwegian Seas on the other, is not condradictory and is also found in present-day SST anomalies (Wallace et al. 1990), and in fully coupled atmosphere-ocean simulations (Delworth 1996). These sea-surface temperature anomalies could play a significant role in the inception of the last glaciation, as they appear before the inception in the palaeo-records. Finally, 115VS is a 45-y long run which includes the SST changes of 115NL and takes the vegetation from the 115V run. This set of experiments has been designed to investigate the separate and combined effects of changes in insolation, vegetation and sea-surface temperature on the ILG climate. None of the experiments has been particularly designed to be more 'realistic' than the others (the imposed SST changes, in particular, are quite crude). Rather, the degree of changes in the components of the climate system other than the atmosphere taken into account in the boundary conditions varies in the experiments, which gives a range of simulations for the climate of the ILG. All the changes will be further illustrated in Sect. 2.3.

2.2.2 Last Glacial Maximum (LGM) experiment

Contrary to the Inception of the Last Glaciation, the Last Glacial Maximum represents an extreme climate change compared to the present-day climate. The CLIMAP (1981) project first estimated global changes in the sea-surface temperatures for this period. The

largest differences were found in the northern high latitudes, with a large SST decrease and sea-ice covering the North Atlantic as far south as 50 °N in winter, whereas the tropical SSTs were not estimated to change much. Although this data set has been criticized over the years (Guilderson et al. 1994; Rind and Peteet, 1985), it was the only comprehensive global data set for the LGM sea-surface temperatures at the time the simulations were performed, in the framework of the PMIP project. Precisely, the SSTs prescribed to the model for the run presented here are built as the sum of the control SSTs and the anomaly between the CLIMAP reconstructions for the LGM and the present climate. They imply a strengthening of the baroclinicity in the Northern Hemisphere winter, especially in the North Atlantic along the sea-ice edge (Hall et al. 1996a, b; Kageyama et al. 1999).

Another important feature of the LGM climate is the presence of large ice-sheets in the Northern Hemisphere mid-latitudes, over what is now Canada (the Laurentide ice-sheet) and Scandinavia (the Fennoscandian ice-sheet). The topography to these ice-sheets has also been evaluated by the CLIMAP project and many of the early simulations of the LGM climate have used this reconstruction (e.g. Manabe and Broccoli 1985; Kutzbach and Guetter 1986; Rind 1987). However, the topography of the ice-sheets has been re-evaluated to lower altitudes (around 2.5 km for the Laurentide ice-sheet and 1.5 for the Fennoscandian) by Peltier (1994) and this latter reconstruction is used in our simulation as in all the PMIP runs. This still represents a large change in albedo as well as in topography (the corresponding sea-level decrease equals 105 m).

The LGM insolation is not significantly different from the present one but has also been included in the forcing. The $\rm CO_2$ concentration is set to 200 ppm after the ice-core analysis from Barnola et al. (1987) and Raynaud et al. (1993). Like the CTRL and the 115I and 115VS runs, this simulation is 45 y long, after the spin-up year.

2.3 Past climate simulations: climatological averages

Here, we examine the anomalies between the climatological averages of the past climate simulations 115I, 115V, 115N, 115NL, 115VS and LGM and the present-climate CTRL simulation. All the results are shown for the winter season and the North Atlantic sector (80 °W-40 °E, 30 to 70 °N), for which the weather regimes are presented in Sect. 3. Figure 2 shows the surface air temperature anomalies. A winter continental warming of around 1 to 3 °C is present in all the ILG simulations, only tempered by a severe cooling (of order 5 °C) over Scandinavia in the 115N, 115NL and 115VS simulations, reflecting the considerable cooling of the Norwegian Sea SSTs. In the 115NL and 115VS simulations, where the Labrador Sea is warmer, the surface air temperatures over the east Atlantic increases by more than 1.5 °C, thus revealing the changes in SSTs imposed on the ocean. The baroclinicity of the flow, as seen through the meridional temperature gradients, is therefore increased a little over the northwestern coasts of Europe in all the runs, but more significantly in the runs where SST anomalies have been imposed. This could give way to a storm-track tail orientated more northeastward towards Iceland than at present. In contrast, the LGM climate is everywhere much cooler than the present day, due to the presence of the ice-sheets over the continents and of the extensive sea-ice over the mid- and high-latitude North Atlantic. The maximal cooling is of more than 25 °C over Iceland (note the different scale for the ILG and LGM surface air temperature figures) and the baroclinicity is enhanced along the sea-ice edge across the Atlantic Ocean, which imposes a more zonal storm-track, as will be shown subsequently.

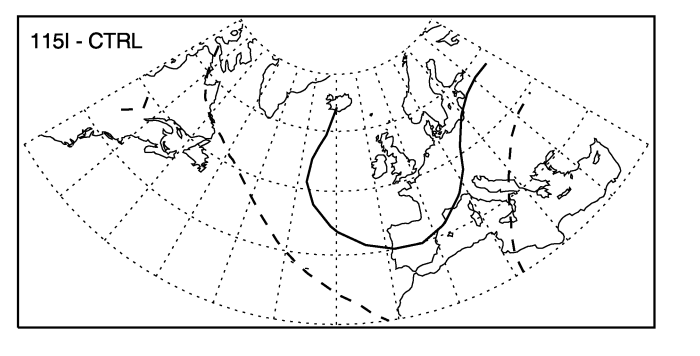
The anomalies in z500 (Fig. 3) roughly follow those seen in the surface air temperature. The ILG simulations are characterized by a positive anomaly above the European west coast, which is larger for the stronger forcings, i.e. those which include changes in the

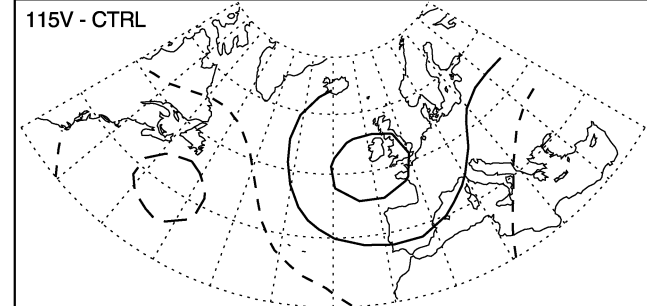
SSTs (115N, 115NL, 115VS). This suggests a more anticyclonic situation over Western Europe, but the changes are not very large. In Sect. 4, the study of the weather regimes in these simulations allows us to assess whether this change is corroborated by e.g. an increase of the frequency of the blocked regime. This anticyclonic anomaly would again favour a northeastward route of synoptic perturbations, as seen in Lau (1988) or Dole (1986). The z500 anomaly of the LGM simulated climate is consistent with the considerable cooling of the North Atlantic sea-ice: a very large negative anomaly dominates the North Atlantic north of 40 °N, accompanied by a positive anomaly to the south of the sector, which is quite large over the Mediterranean. This implies a strengthening of the jetstream across the Atlantic Ocean, which again favours a more zonal storm-track. The same scale is used for the ILG and the LGM experiments, which clearly shows the differences between the amplitudes of the anomalies for these periods.

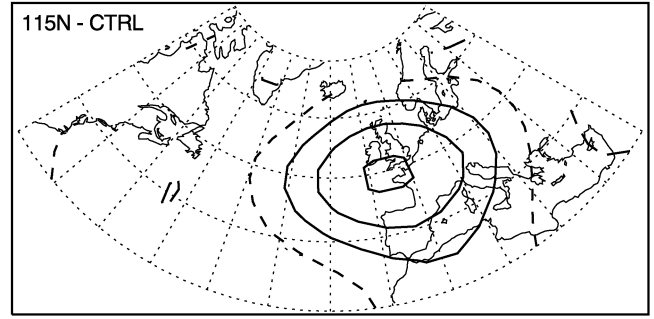
Figure 4 shows the anomalies in the high-pass filtered z500 standard deviation, which gives a measure of the storminess in the sector, again with the same scale for all simulations. The changes in the ILG storm-tracks compared to the control run are quite subtle, with a hint of a decrease over the central and eastern Atlantic and central and southern Europe and a hint of an increase over the Norwegian Sea and Scandinvia, in the 115I and 115V runs. These tendencies are confirmed in a more convincing manner in the 115N, 115NL and 115VS runs and this northward shift of the tail of the storm-track is consistent with the changes seen in the surface temperatures and the z500 anticyclonic anomaly. As for the other fields, the LGM anomaly in storminess is very strong compared to the ILG ones and shows a marked eastward shift and strengthening of the storm-track, which is consistent with the changes in baroclinicity.

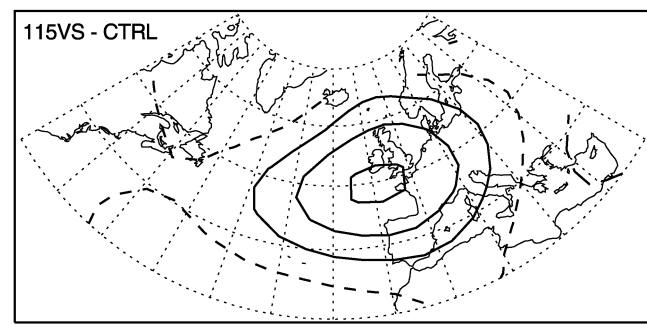
Finally, Fig. 5 show the percentage precipitation change for the different runs. A feature common to all the ILG runs is the decrease in precipitation over the eastern Atlantic and southern Europe, which is consistent with the z500 anticyclonic anomaly and the northward shift of the tail of the storm-track. In the runs for which the SSTs have been changed (115N, 115NL, 115VS), this also leads to an increase of precipitation over northern Europe. However, the signal is difficult to extract in this region because it is represented by a very few points in the model since its latitudinal grid is regular in sine of the latitude. In the 115NL and 115VS runs, there is also an increase of the precipitation over the western Atlantic above the warm anomaly imposed in the model. This is most likely due to the additional energy available to the atmosphere from the warmer ocean, which does not affect the storm-tracks strongly (Fig. 4) but shows a more direct response in the precipitation field. The anomaly is very localized over the ocean and is small over the site of growth of the Laurentide ice-sheet. At the LGM, the opposite effect is evident over most of the sector, with a decrease of precipitation due to the colder temperature, despite the strengthening of the stormtrack. In fact, over the eastern side of the Atlantic, where the strengthening is largest, there is a slight increase in precipitation.

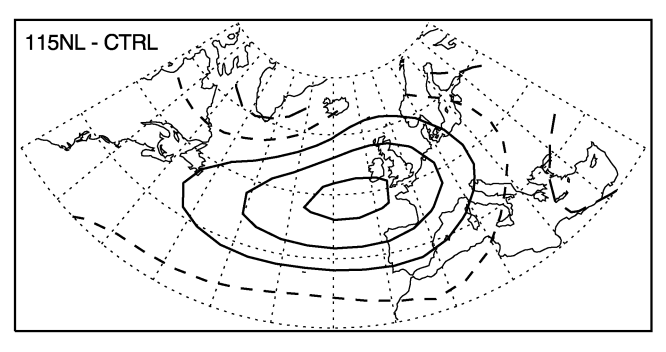
The climatological averages for the present-day and past climate simulations give us a first idea of the differences between the climates. The atmospheric circulation changes appear to be consistent with the forcing imposed on the model and the surface air temperature changes, while the precipitation changes are related not only to the circulation changes but also to the air temperatures, especially in the LGM case. The differences in the ILG mainly consist of an anticyclonic anomaly over the eastern Atlantic and Western Europe, consistent with a northward shift of the tail of the storm-track and a drying over Western Europe and the east Atlantic. Even in the runs in which larger forcing changes have been applied, they remain quite small compared to the differences between the CTRL and the LGM climates (they are nevertheless statistically significant over most of the domain, which is not shown here for clarity of the figures). The circulation at the LGM is stronger and more zonal, accompanied with an eastward shift and strengthening of the stormtrack. This is only partially translated into precipitation changes, due to much colder temperatures.











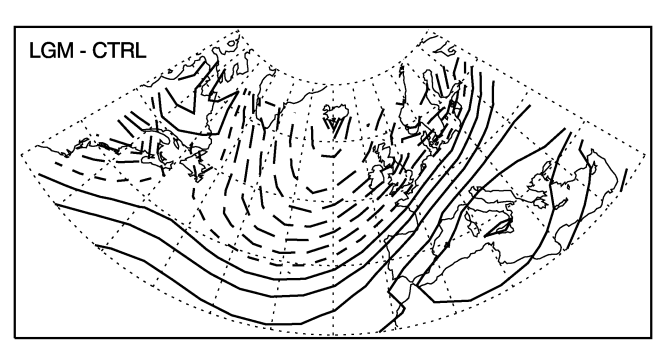


Fig. 3 Anomalies in 500 hPa geopotential height between past climate DJF climatological means and the control one. *Top-left*: 115I, *top-right*: 115V, *middle-left*: 115N, *middle-right*: 115VS, *bottom-left*:

115NL, bottom-right: LGM. Contours every 20 m from -200 to +200 m, zero contour short-dashed, negative contours long dashed lines

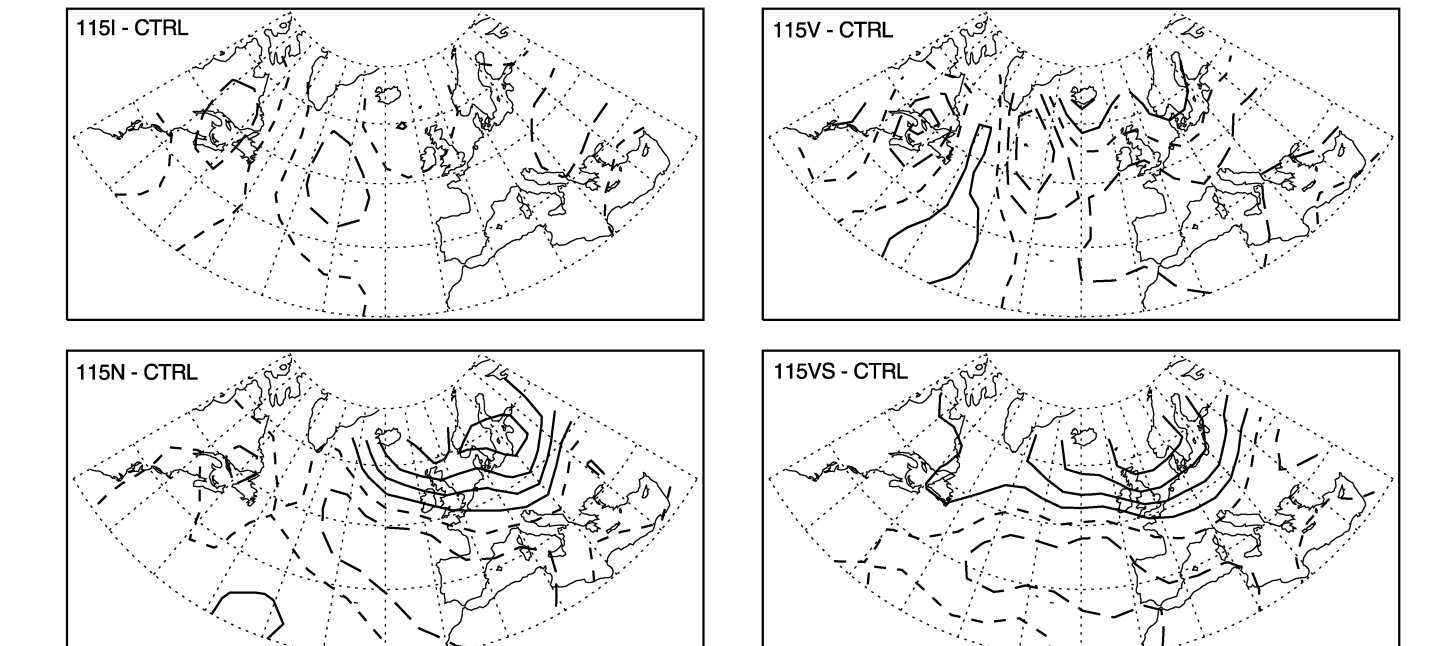
3 Weather regimes in the present climate simulation

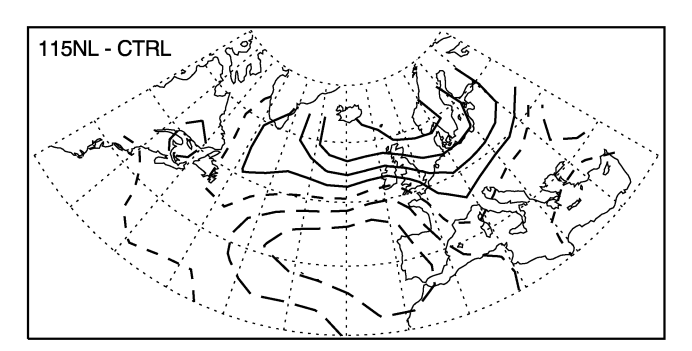
3.1 Cluster analysis

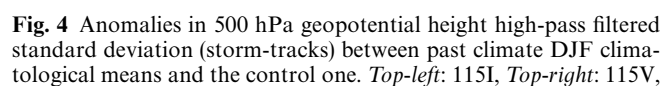
To retrieve the weather regimes from our simulations, we use the clustering algorithm from MVL, with which daily maps of the winter atmospheric circulation can be divided into clusters of similar states. MVL show that the regimes obtained with their method compare well with those, also defined as the most recurrent patterns of the circulation, found by another clustering algorithm (Cheng and Wallace 1993) or by an algorithm looking for maxima in a probability density function of the states in some subspaces of the phase space (Kimoto and Ghil 1993). They also compare the results with regimes defined as quasi-stationary states of the atmosphere (following the method of Vautard 1990). They find the same number of regimes with both

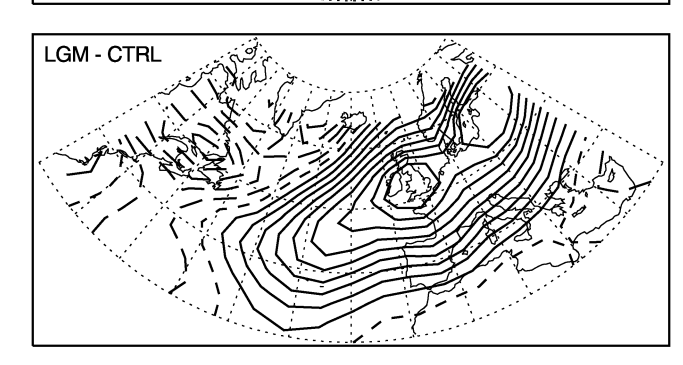
methods, but the regimes do not all correspond, due to the fact that the most recurrent states of the atmosphere are not necessarily quasi-stationary, nor especially persistent. This clustering algorithm has the advantage of being automatic, in the sense that it does not rely on the results for the present climate to infer weather regimes for past climates.

We analyze daily z500 December–January–February data for the same North Atlantic sector as in MVL: 80°W–40°E and 30–70°N. We first subtract the climatological average from the data and work on the anomalies from this average. An EOF decomposition of these anomalies is performed and the projections on the eight leading eigenvectors are retained. These, in all cases, explain more than 80% of the variance. The cluster analysis is performed in this reduced EOF space, before transforming the results back to physical space. The procedure, fully detailed in MVL, is a non-hierarchical algorithm which starts from a set of as









middle-left: 115N, middle-right: 115VS, bottom-left: 115NL, bottom-right: LGM. Contours every 2.5 m from -25 and +25 m, zero contour short-dashed, negative contours long-dashed lines

many random seeds as the chosen number of clusters and recursively converges to a partition that minimizes the sum of variances within clusters. This final partition is in principle independent of the initial set of random seeds.

Based on a test of this independence, MVL devised a classifiability index which determines the best choice for the prescribed number of clusters: the clustering algorithm is run 50 times (we also have checked our results by running it 100 times) from a different initial set of random seeds. The classifiability index is calculated as the average of the pattern correlations (or ACCs, for anomaly correlation coefficients) between the centroids of each partition. The higher the classifiability index, the more similar the 50 (or 100) partitions are. This classifiability index is compared to the results from a reference noise model (first order Markov process), which generates 100 series of the same length as the initial dataset, with the same covariances at lags

0 and 1 days as the data set. The classifiability index is calculated for each of these 100 samples and the upper and lower bounds of confidence are assigned to the 10th highest and 10th lowest values of these indices. Figs. 6 and 13 show the classifiability indices and these two bounds for the CTRL and LGM simulations. The best choice for the number of clusters is the one for which the differences between the data classifiability index and the upper bound of the confidence interval is highest.

3.2 Simulated present-climate weather regimes

The cluster analysis has been performed with a prescribed number of 2 to 8 clusters on the present-day 45-winter daily data and the most and only classifiable case has been found for four regimes (Fig. 6), as found by MVL for the observed daily 700 hPa geopotential

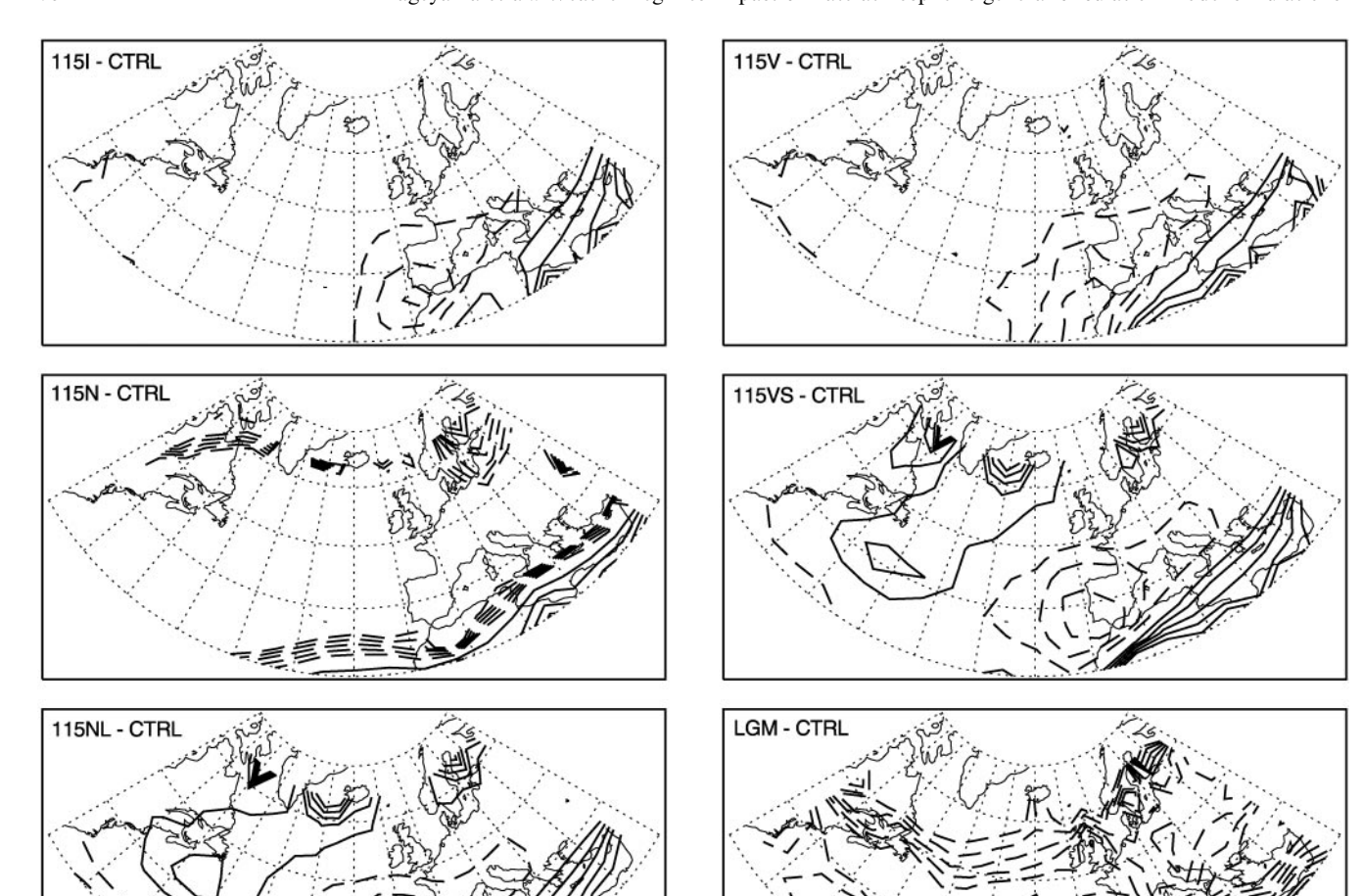


Fig. 5 Precipitation change, in percent, between the control and the past climate DJF climatological averages, *Top-left*: 115I, *top-right*: 115V, *middle-left*: 115N, *middle-right*: 115VS, *bottom-left*: 115NL,

bottom-right: LGM. Contours every 10% from -50 to 50%, zero contour omitted, negative contours dashed. The field has been filtered for clarity

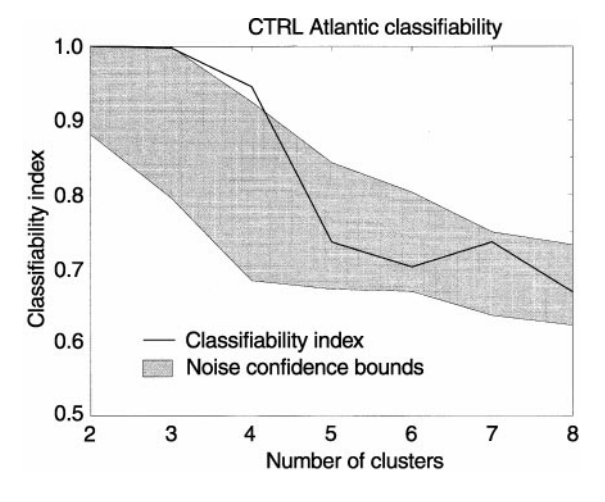
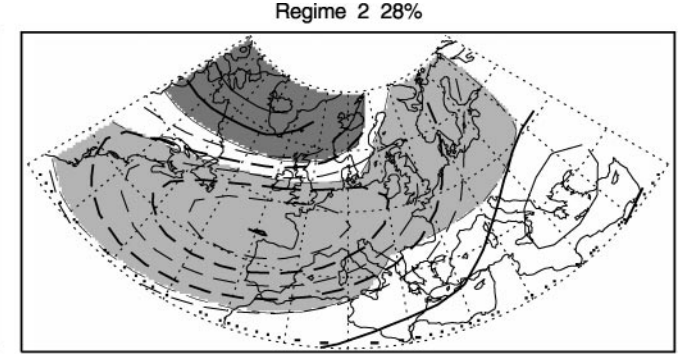


Fig. 6 Classifiability index (thick line) and confidence interval (thin lines) for this index (see text and MVL for details) for the control run, as a function of the number of clusters

heights. Figure 7 shows the z500 anomalies for the centroids of the four regimes. For comparison, we have also computed the classification of the NCEP re-analyses data (four times-daily z500 data from January 1980 to December 1995) into four regimes. This gives a better element of comparison for our results, since MVL's clusters are computed from the 700 hPa geopotential height. The first regime consists of a positive z500 anomaly over the eastern Atlantic accompanied by a negative anomaly over southwest Europe, similar to MVL's "Atlantic ridge" regime (their Fig. 4d). Compared to the corresponding NCEP regime, the trough to the east of the ridge is situated too much to the southwest, but the ridge itself is well located. The second regime corresponds to a high over Greenland and a low over most of the Atlantic basin. It corresponds to a southward shift of the jet-stream. It is similar to MVL's first regime (their Fig. 4a) and has a powerful projection on the North Atlantic oscillation

Regime 1 23%



Regime 3 28%

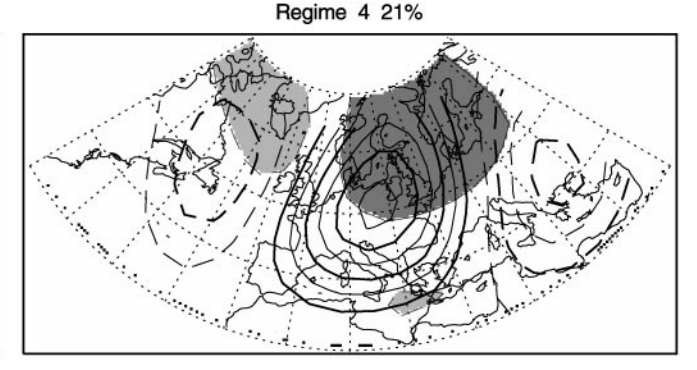


Fig. 7 Cluster centroids found for the CTRL experiment is for the NCEP re-analyses (1980–1995). The variable plotted as the 500 hPa geopotential height anomaly from the climatological average of the given data set. The contours (every 20 m from -200 to +200 m, 0 contour omitted, dashed contours for negative

values) show the results for the CTRL simulation. The areas with dark and light shading show the results for the NCEP re-analyses: dark shading for values larger than 40 m, light shading for values smaller than -40 m

pattern (Wallace and Gutzler 1981). Its structure compares well to the one computed from the NCEP re-analyses. The third regime, on the contrary, corresponds to a northward shift of the jet-stream, and would resemble MVL's zonal regime (thier Fig. 4c). However, the NCEP positive anomaly to the south of the sector is small compared to ours. The fourth regime is characterized by a strong positive anomaly over Western Europe, surrounded by two negative anomalies to the east and to the west, and can be interpreted as being the model's representation of the blocking regime, which is located southwestward from its observed position over Scandinavia. Given the fact that the storm-track is weaker and shorter than observed, and that the lowfrequency variability is largest at the end of stormtracks (Blackmon et al. 1977), this misrepresentation of the blocking regime in the model is plausible. This phenomenon has also been reported in higher resolution models (Carnell et al. 1996; Ferranti et al. 1994a). Therefore the simulated weather regimes are realistic enough to be compared to the observed ones, which confirms that they are more dependent on the internal dynamics of the atmosphere than on the interannual variability of the boundary forcing.

The local weather associated with each of the regimes can be described by calculating the composite average of the surface air temperature, storminess and precipitation over each of the clusters. The patterns in z500 for each regime are easily recognizable in the surface air temperature, Fig. 8. The z500 anomalies are located westward from the temperature ones and one can explain, for example, the cold anomaly over Europe in the fourth regime as being the result of the advection of cold air by the anticyclonic anomaly situated over the European coast. The structure of the temperature anomalies given on Fig. 8 compare very well with MVL's 850 hPa temperature composites (their Fig. 16).

Figure 9 shows the high-pass filtered z500 standard deviation anomalies composited for each regime. The storm-tracks follow the changes in the mean flow, consistently with the results of Lau (1988) and Fraedrich et al. (1993) on monthly time scales, and of Dole (1986) on the shorter time scales of his persistent anomalies: in the second regime, both the jet-stream and the storm-track are shifted southward, contrary to the third regime where they are shifted northward. In the fourth regime, the tail of the storm-track is shifted northward and the beginning of the storm-track

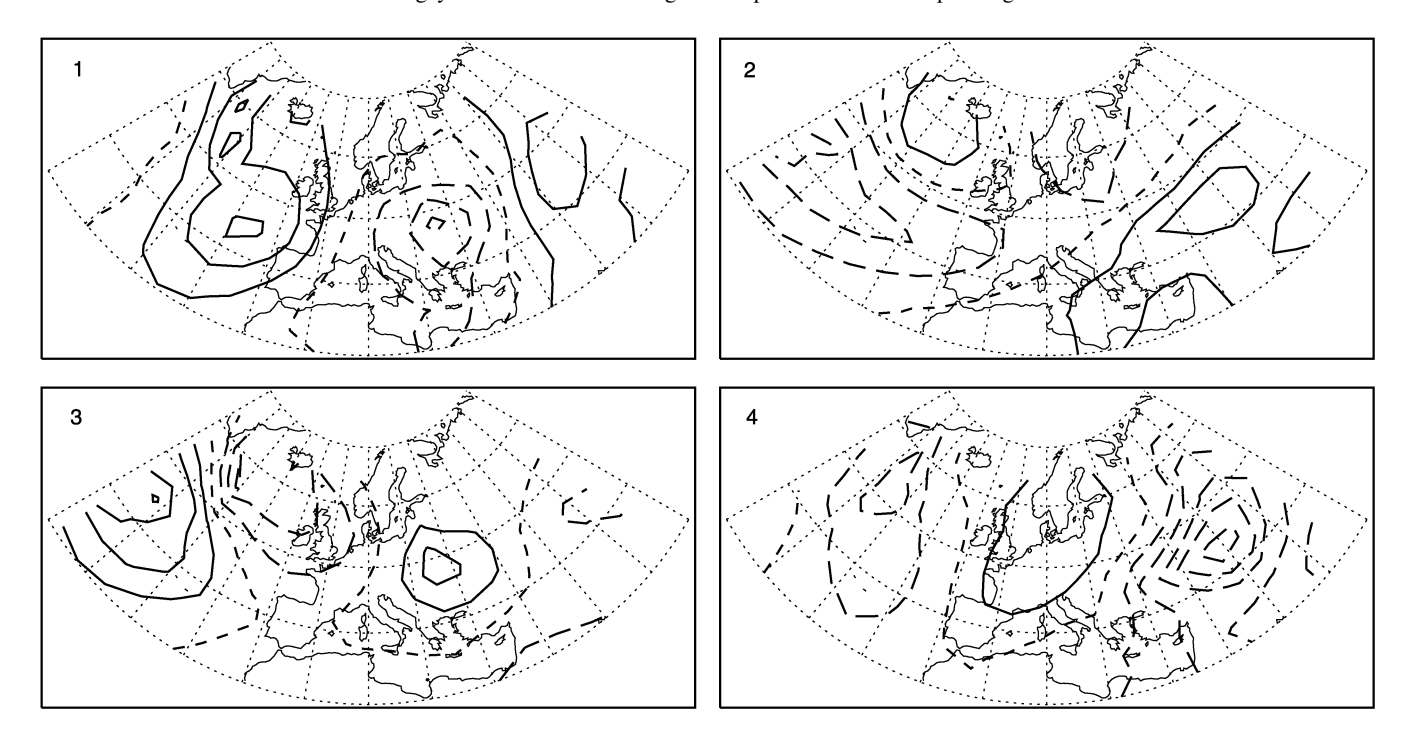


Fig. 8 Surface air temperature anomalies from the climatological average, composited on the four clusters of the CTRL experiment shown in Fig. 7. Contours every 1 $^{\circ}$ C from -10 to +10 $^{\circ}$ C, zero contour short-dashed, negative contours long-dashed lines

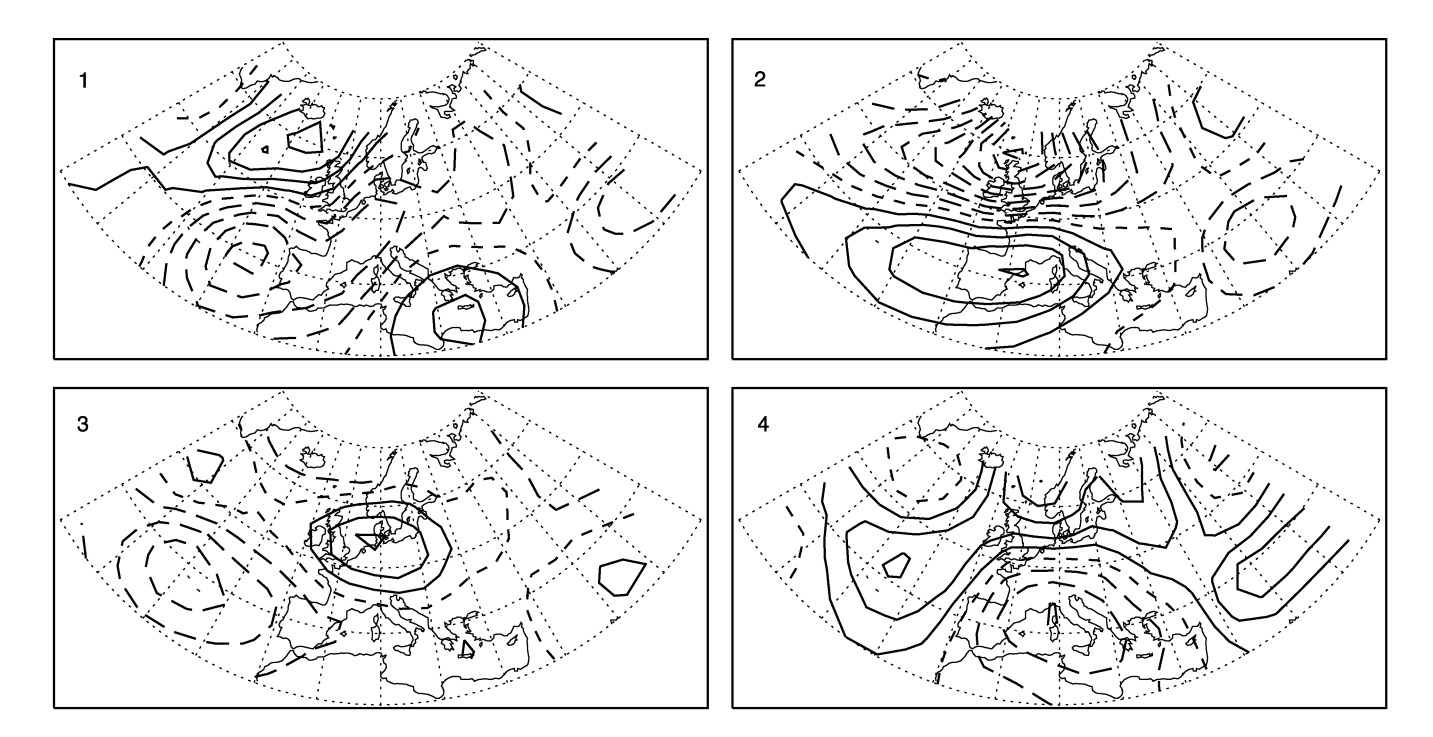


Fig. 9 500 hPa geopotential height high-pass filtered standard deviation (storm-tracks) anomalies, composited on the four clusters of the CTRL experiment shown in Fig. 7. Contours every 2.5 m from -25 to +25 m, zero contour *short-dashed*, negative contours *long-dashed-lines*

strengthens, consistently with synoptic studies on the behaviour of high-pass filtered transient eddies during blocking epidodes (Nakamura and Wallace 1990). The changes in the first regime are more complicated but are also consistent with the mean flow anomalies, with a northward shift of the storm-track and the jet-stream over the eastern part of the sector and their southward shift over Western Europe.

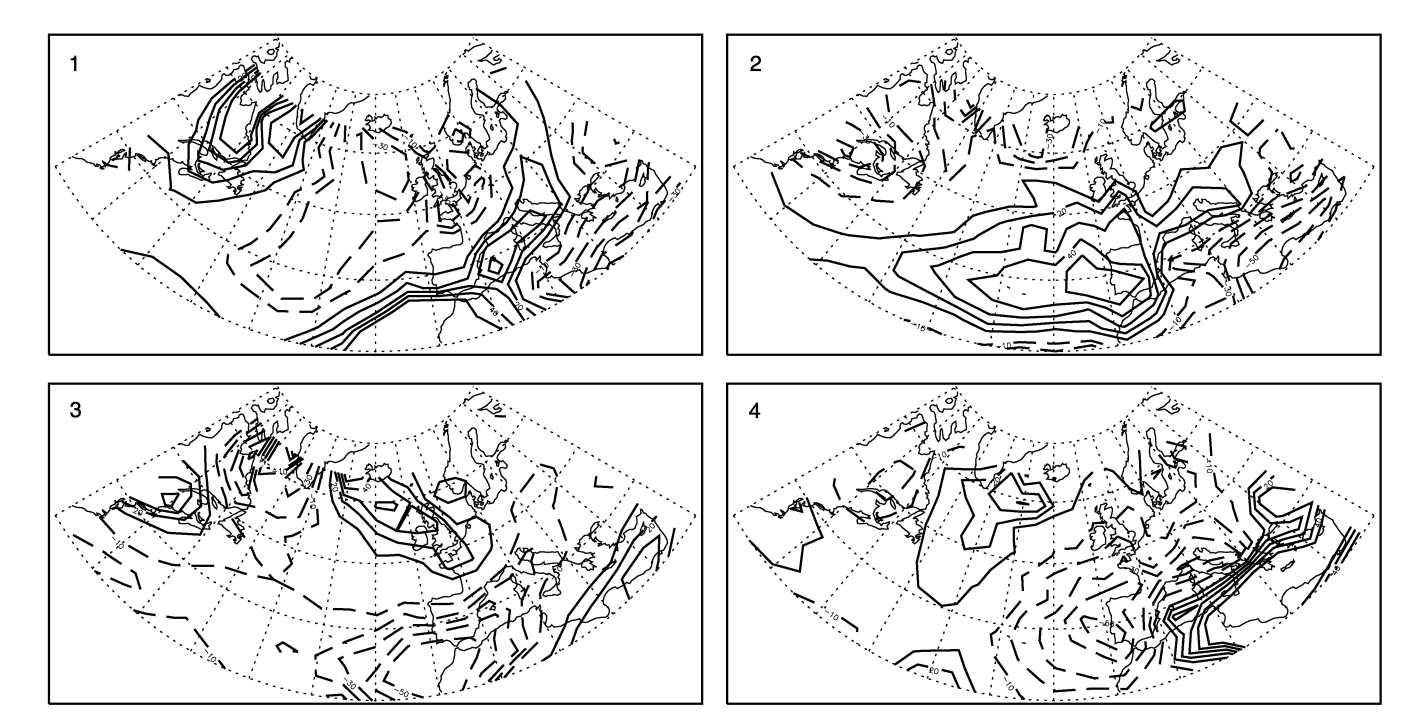


Fig. 10 Precipitation, composited on the four clusters of the CTRL experiment shown in Fig. 7. The change compared to the climatological average is shown in %, with contours every 10% from -50 to +50%, negative contours dashed, 0 contour omitted

The corresponding precipitation anomalies, shown on Fig. 10 as the percentage of difference compared to the climatological average, are consistent with the storminess anomalies. In particular, the second regime is characterized by an increase of precipitation over southern Europe and a decrease over the ocean and northern Europe, which correlates well with the southward shift of the storm-track. On the contrary, the fourth regime is characterized by an increase of the precipitation over northern Europe and a decrease over southwestern Europe. It is interesting to see that determining our regimes only from the daily anomalies in the 500 hPa geopotential height and then retrieving the weather characteristics of each regime by compositing the surface air temperature, storminess and precipitation over the clusters constituting the regimes, we find patterns very similar to Fraedrich et al. (1993), who analyzed the 100-y-long time series of a vector containing altogether the monthly averaged normalized meansea-level pressure, surface temperature and precipitation for 40 European stations. This shows very clearly the link between local weather and large-scale lowfrequency variability.

4 Weather regimes in the past climate simulations

4.1 Cluster analyses

The same cluster analysis as for the present-day run has been performed on the z500 daily fields from our long

past climate simulations: 115I, 115VS and LGM. In the first two cases, the same number of regimes as for the present-day has been found (classifiability indices not shown). The centroids for these regimes are displayed in Figs. 11 and 12. They are very similar to the present-day clusters, with slight modulations over the eastern part of the domain for regimes 2 and 3, and over the western part of the domain for the fourth regime in simulation 115VS.

It is therefore interesting to compare the populations of the weather regimes in the CTRL, 115I and 115VS runs. These are given in Table 2. In the 115I case, there is a significant decrease of the population of the second regime, compared to the present situation. This is the regime where the jet-stream, storm-track and main precipitation are high in the south of the domain. This decrease in the population of the second regime is compensated by an increase in the third and fourth regimes, where the storminess is highest over northern Europe. The differences are larger between the 115VS and the CTRL weather regime populations: while populations of regimes 1 and 3 are stable, there is a large increase in the fourth regime and a corresponding large decrease in the second regime. Both changes show that a northward position of the storm-track is favoured in this simulation, as is the case in the 115I experiment.

The fact that regime 4 is favoured at the expense of regime 2 can be explained as follows: in terms of the 500 hPa geopotential height, the ILG insolation forcing can be thought of as imposing a positive anomaly over the

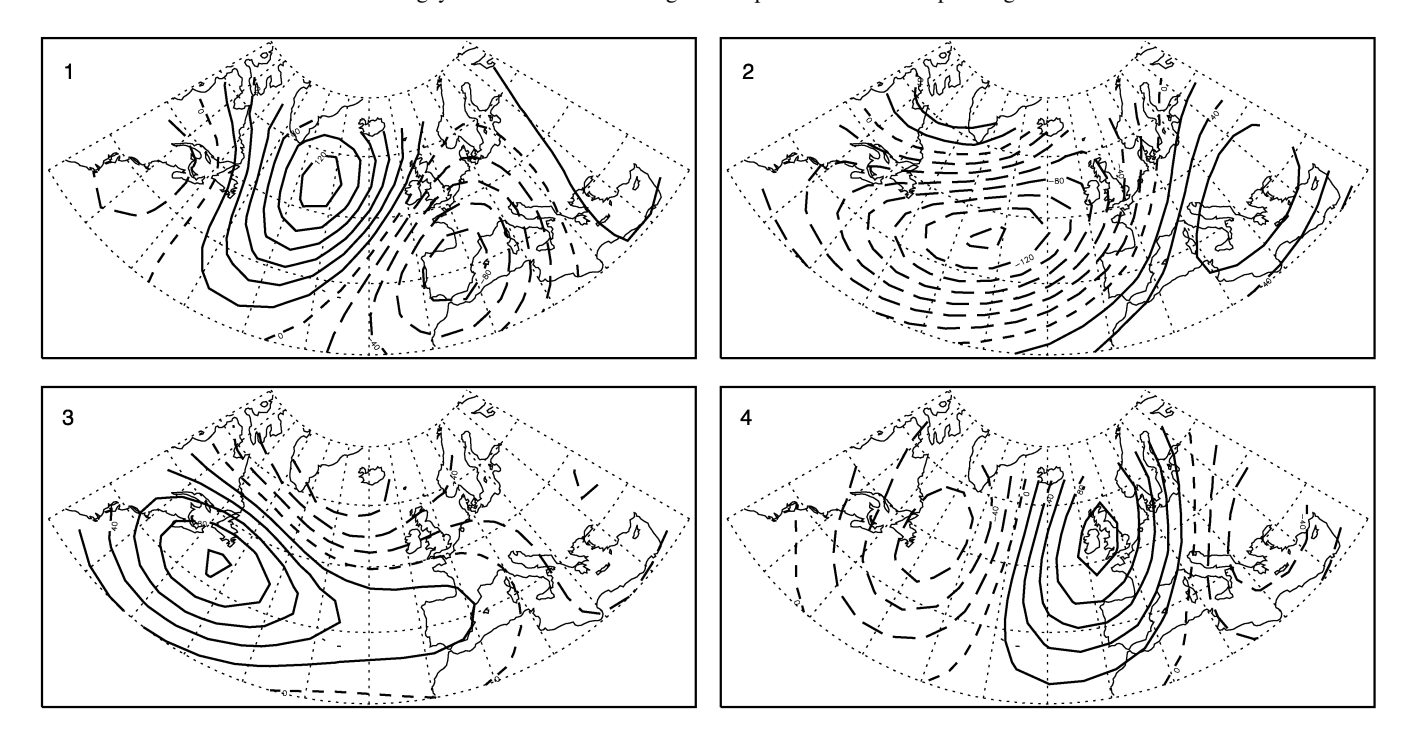


Fig. 11 Clusters centroids found for the 115I experiment. The variable plotted is the 500 hPa geopotential height anomaly from the 115I climatological average. Contours every 20 m from -200 to +200 m, zero contour short dashed, negative contours long-dashed lines

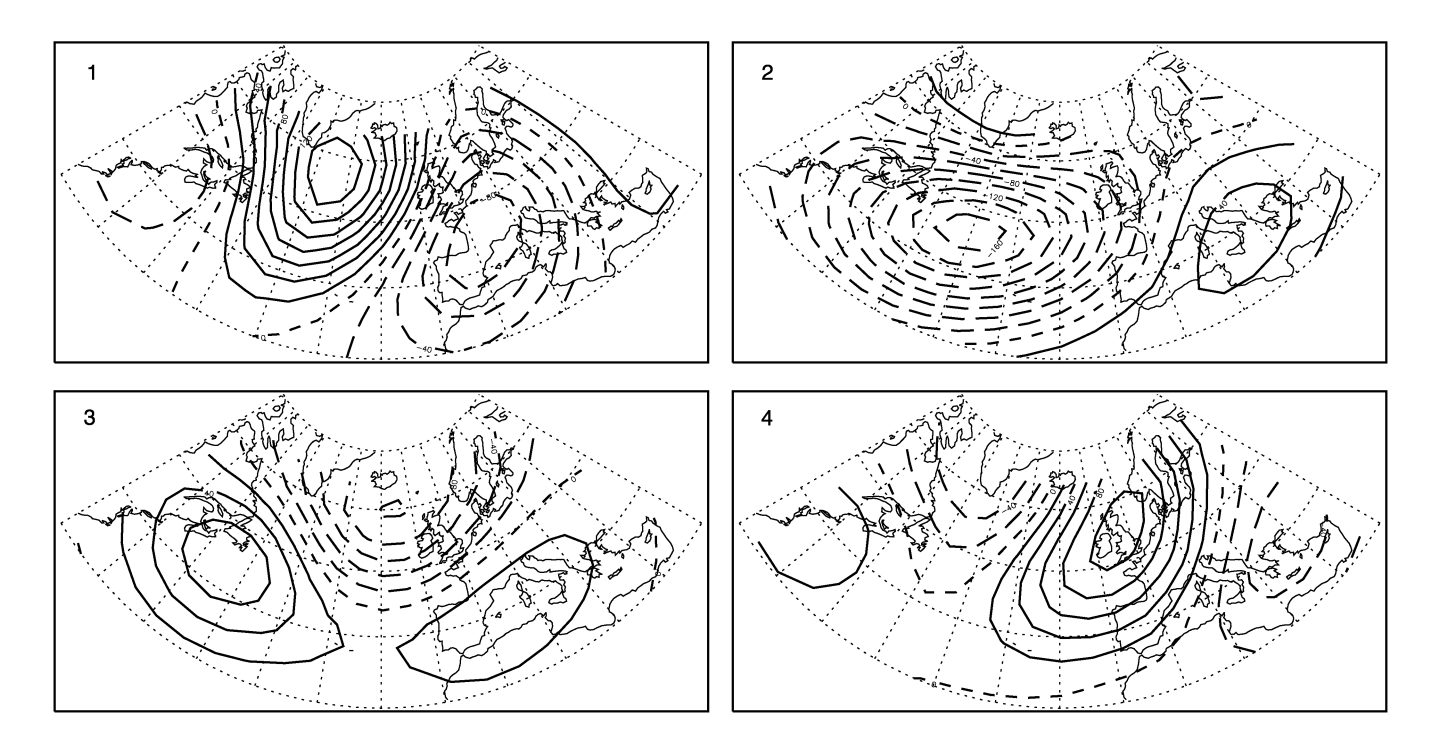


Fig. 12 Cluster centroids found for the 115VS experiment. The variable plotted is the 500 hPa geopotential height anomaly from the 115VS climatological average. Contours every 20 m from -200 to +200 m, zero contour short-dashed, negative contours long-dashed lines

continents, i.e. mainly Europe in our case. Also, the additional SST forcing over the Norwegian Sea implies a strengthening of the meridional gradient of temperature and z500 over the northeastern Atlantic and

northern Europe and, as a consequence, an enhancement of the anticyclonic anomaly over Europe. The regime which has the strongest positive z500 anomaly over Europe is regime 4. Conversely, regime 2 consists

Table 2 Percentage of days in the four weather regimes in Fig 7, 11 and 12

Simulation	Regime 1 (%)	Regime 2 (%)	Regime 3 (%)	Regime 4 (%)
CTRL	23	28	28	21
II5I	23	23	30	23
115VS	22	20	29	29

of a strong z500 negative anomaly over the major part of the domain. Therefore, in the case of the ILG climate, the regime which is favoured is the one on which the forcing projects better, at the expense of a regime which contrasts with this forcing.

This increase in the population of the fourth regime and decrease in the population of the second one also faithfully describe the northward displacement of the major zones of storminess and precipitation (compare Figs. 3 and 9 for the storminess and Figs. 5 and 10 for the precipitation). The changes in surface air temperature are more difficult to understand and do not correspond directly to the forcing, particularly in SSTs (compare Figs. 2 and 8). This illustrates, as pointed out by Palmer (1993), that changes associated with weather regimes can be counter-intuitive.

Overall, the weather regimes appear to be a good tool, in the ILG case, to describe concisely and also more precisely the differences of the climate compared to the present one. Our results for the ILG simulations therefore agree with the ideas of Ghil and Childress (1987) and Palmer (1993, 1998) reported in the introduction and show the non-linearity of the climate changes between these two periods. Indeed, while linear thinking, as explained by Palmer (1993), would suppose a change in the climatological average without significant changes of the variability around this mean, non-linearity is marked by changes that affect differently each of the regimes, which can explain a change in the mean climate, since this climate can be defined as the weighted average of the weather regimes.

The LGM simulation differs from all the others by the fact that for this simulation, the classifiability index (Fig. 13) always lies within the bounds of what could be explained by red noise signals, for all the numbers of clusters considered. Therefore, no significant number of clusters could be found at the chosen significance threshold. (The confidence level for the classification of the CTRL maps in 4 clusters is 93%, higher than for any other number of clusters between 2 and 8. This level reaches 99% for 115I and 98% for 115VS. For the LGM simulation, the best confidence level obtained for the classification is 84%, for 5 clusters, which is much lower than the highest confidence level obtained for the CTRL and 115I results.) In fact, we show in Sect 4.3 that the low-frequency variability of the LGM atmosphere is not dominated by persistent, recurrent

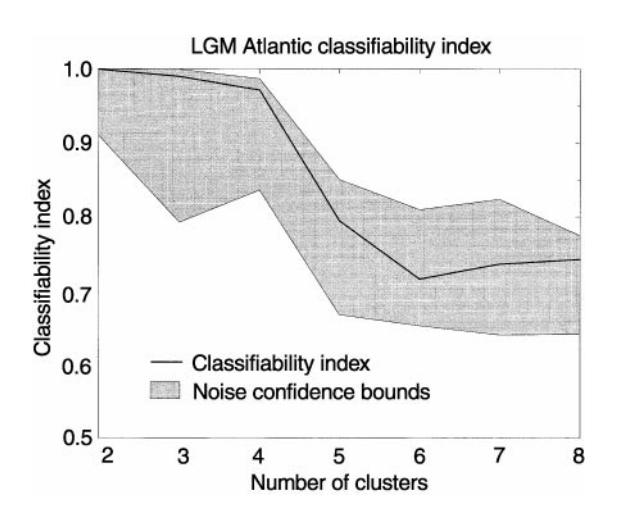


Fig. 13 Classifiability index and associated confidence interval, same as Fig. 6 but for the LGM simulation

anomalies, but rather by large-scale oscillations. This shows that there are cases where weather regimes cannot be defined, which excludes an analysis of climate differences in terms of variations in the weather regimes populations, as we developed for the ILG climate.

4.2 Analyses using the weather regimes of the control experiment

Before investigating further the LGM case, we want to examine whether we can use the classification from the present-day simulation to describe the past climate changes in our simulations. For this, we have classified the data from our past climate simulations within the boundaries of the clusters defined from the CTRL experiment. This implies taking the anomaly from the present-day climatological average, projecting these anomalies on the present-day eight leading EOFs and classifying these projections according to the present day regimes by assigning a map to the closest centroid in EOF space. Table 3 gives the populations of the regimes for all our climate runs. For the 45-y-long runs, the weather regime populations have also been calculated for the first, second and third 15-y periods of the run to estimate the variability of populations along the simulations. The populations of the regimes for each 15 y prove to be quite variable (see e.g. the presentday regimes 2 and 4) but the results reported subsequently are robust. Futhermore the results for the control run CTRLV using the 17 biome version of the AGCM (see Sect. 2.1) are in the range of the regime populations of the CTRL run, which confirms their similarities.

In the ILG simulations, the most robust features are the increase of the population of the fourth regime, from less than 25% to more than 30% in all the ILG runs and the decrease in the population of the second

Table 3 Percentage of days belonging to the four weather regimes of the control experiment (Fig. 7). See text for details on how these percentages are obtained. Results labelled EXPERIMENT/1,2 or 3 refer to the first, second or third 15 y of a 45-y-long simulation

Simulation	Regime 1 (%)	Regime 2 (%)	Regime 3 (%)	Regime 4 (%)
CTRL CTRL/1 CTRL/2 CTRL/2	23 25 23 20	28 23 25 36	28 29 28 27	21 23 24 17
CTRLV	26	23	28	23
115I 115I/1 115I/2 115I/3	22 24 20 22	23 20 23 26	24 24 23 23	32 32 34 30
115V	20	26	22	33
115N	15	22	27	36
115NL	20	12	33	34
115VS 115VS/1 115VS/2 115VS/3	20 19 20 22	16 13 20 16	29 31 29 28	34 37 32 35
LGM LGM/1 LGM/2 LGM/3	9 9 10 7	46 41 50 50	35 39 28 37	9 11 12 7

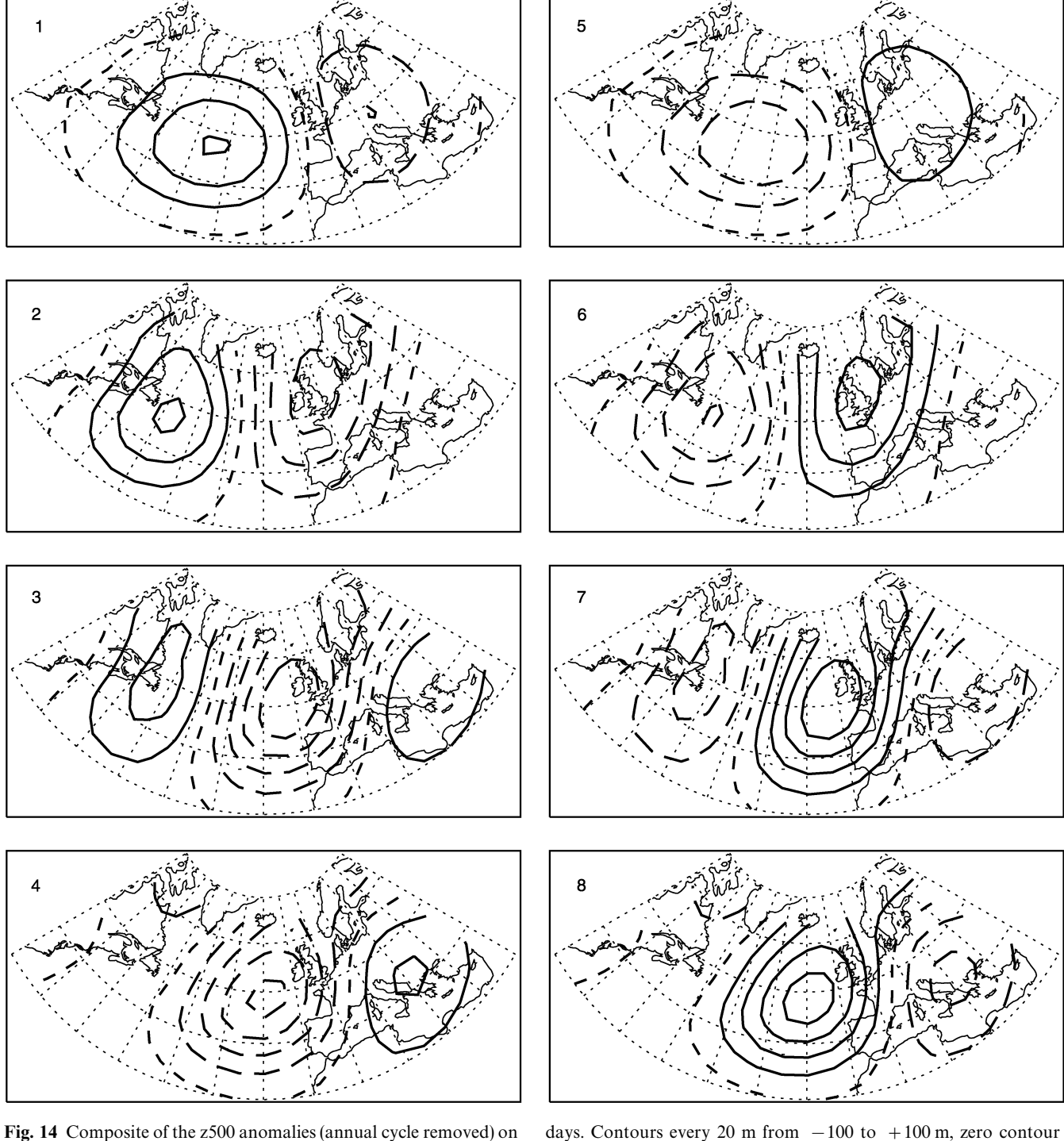
regime, which is largest (from 28% to 12% and 16%) for the 115NL and 115VS experiments, in which the largest boundary forcing have been applied. As discussed in the previous section, these changes are another way of analysing the northward shift to the jet-stream, precipitation, and storm-tracks in these simulations. The changes here are larger than those seen in the previous section for 115I and 115VS, in which the regimes were re-calculated and hence could somewhat slightly "adapt" to the changes in boundary forcing.

In the LGM case, the data is mostly partitioned between the second and the third regimes. Going back to Fig. 3, one can see that it is mainly the difference in climatological averages that is projected on the two regimes: these are the only ones to display a negative anomaly to the north of the sector, which is the major feature of the difference between the LGM and presentday climates. In fact, if composite maps are made from the ILG simulations that are classified within each CTRL cluster, the same patterns are found as for the present day (not shown). On the other hand, the composites obtained in the same manner from the LGM data do not yield the same patterns, which shows that the CTRL weather regimes are not a good basis to represent the LGM climate. This shows the limit of this approach. It suggests that this method cannot be used for extreme climates whose climatologies are far from the control one and whose fields, composited using a classification between the present-day regimes, do not give the patterns characteristic of these regimes.

4.3 A low-frequency oscillation in the LGM case

The previous subsections showed that the low-frequency variability of the LGM atmospheric circulation could not be characterized in the same way as for the present-day or the ILG cases. This deserves a complementary analysis. First, the leading two EOFs describe a very large part of the variance (25% for the first EOF, 20% for the second) compared to the CTRL (for which the first two EOFs explain 35% of the variability), the 115I (35%) or the 115VS (34%) simulations. This suggests quite a simple behaviour in phase space, with variability taking place mainly in the subspace of the first two EOFs. We investigate further in this direction by performing a multi-channel singular spectrum analysis (MSSA), a tool that isolates the main oscillations of the flow, which explain a large part of the atmospheric variability. MSSA analyzes time series of vectors constituted, for a given day, by the sequence of the map for this day and the M-1 following maps. M is called the window length. The analysis consists in a principal component analysis of these vectors, i.e. in the diagonalization of the lagged covariance matrix. The eigenvectors of this matrix are in turn lagged sequences of maps, and are called ST-EOFs (space-time EOFs). Similarly to classical principal component analysis, ST-PCs are defined as projections of the original series on the ST-EOFs. Plaut and Vautard (1994) showed that pairs of very close eigenvalues in the spectrum of the matrix which correspond to pairs of ST-EOFs and ST-PCs in phase quadrature define an oscillation in phase space. The reader is referred to Plaut and Vautard (1994) for theory and application of this method.

We have analyzed the daily z500 for the whole 45 annual cycles of our CTRL and LGM simulations; the mean annual cycle was subtracted from the signal, no additional filtering has been applied. The analysis has been conducted in the subspace of the 5 to 8 leading spatial EOFs. Both for the CTRL and LGM simulations, the results are stable with respect to the number of EOFs retained and window lengths chosen (100, 150 and 200 days). For the CTRL, two main propagating structures are found, very similar to those retrieved from the NCEP re-analyses by Plaut and Vautard (1994). This type of low-frequency variability is therefore well represented in the AGCM. For the LGM, the most robust oscillation is an eastward propagating wave of period 40–50 days, which explains around 35% of the variance in that frequency band, which compares well to the percentages found in Plaut and Vautard (1994) in their observational study. There is no other type of robust oscillation. The results for the LGM are therefore very



the phases of the pair 4–5 oscillation recovered by MSSA decomposition on the leading 8 LGM EOFs, using a window length of 100

days. Contours every 20 m from -100 to +100 m, zero contour short-dashed, negative contours long-dashed lines

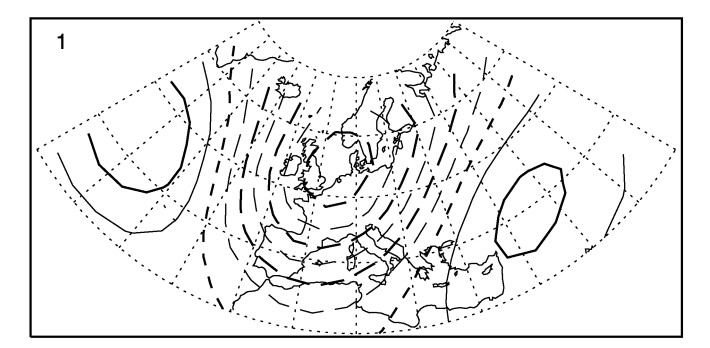
different from the results from the CTRL, with a simple, single-oscillation-type low-frequency variability.

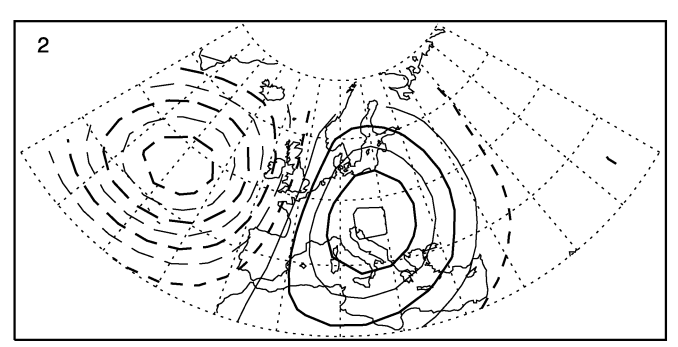
A phase composite of the z500 anomalies on this oscillation is shown in Fig. 14. To compute this composite, the phase of the oscillation is first defined starting from the pair of space-time PCs that has been found to give rise to the most significant oscillatory pattern.

The phases are calculated for every day of the simulation and then divided into eight categories of equal populations. The composite averages are computed for each of these eight cateogries, finally showing the pattern and evolution of the oscillation (for more details, see Plaut and Vautard 1994). In the present case, the oscillation consists of a retrogressing large-scale

(around wave number 6) pattern. The propagation is very zonal, showing the strong constraint of the thermal gradient induced by the sea-ice edge across the Atlantic. This zonal constraint therefore appears to "simplify" the dynamics of the the low-frequency variability. This type of retrogressing pattern has been found in the present-day circulation over the Pacific (Kushnir 1987; Ghil and Mo 1991), which gives us confidence in the fact that it could also occur in our LGM circulation, characterized by strong baroclinicity and jetstreams and a modified topography. Marcus et al. (1994) have indeed shown that variability on these time scales was linked to the interaction between the flow and the topography and that it does not occur in simulations with a flat surface. However, the mechanism explaining this retrogressing oscillation remains to be precisely explained.

It is possible that the low-frequency weather-regimelike varibility is shifted to the east along with the storm-track but out of the sector studied here. We have performed a cluster analysis on a sector shifted to the east by 30°. Using the same criteria as for all other simulations, the data proves to be classifiable into three regimes, although by a very short margin (confidence level: 90%). The patterns of these three regimes (Fig. 15) strongly resemble some of the phases of the oscillation shown in Fig. 14: regime 1, with a deep low over Western Europe, is similar to phase 2, regime 2, with a low over the east Atlantic and a high over central Europe, is similar to phase 5, and regime 3 resembles phase 7. To verify that these weather regimes and the low-frequency oscillation are indeed linked, we have first computed the time of residence of each regime in the different phases of the oscillation. Figure 16 shows that the occurrence of regime 1 is maximal in the second phase of the oscillation, a maximum of days in regime 2 occurs in the fifth phase of the oscillation, and in the seventh phase for regime 3. Second, we have computed the number of transitions between the three regimes, for episodes of duration larger than 5 days (Table 4). The transitions from regimes 1 to 2, 2 to 3 and 3 to 1 are more numerous than those from regimes 2 to 1, 3 to 2 and 1 to 3, respectively. This suggests that a propagation from regime 1, to 2, and then 3, which is the one found independently through the MSSA of the same data, is favoured compared to propagation in the opposite direction. To check the statistical significance of this result, we have followed the method described by Vautard et al. (1990), and have computed the number of transitions in a Monte-Carlo ensemble of 1000 elements (computed in the same way as to determine the classifiability of the data into clusters). Table 5 shows that transitions from regime 1 to regime 2 and from regime 2 to 3 are robust at 99.9 and 93.4% levels of confidence. The next most robust transition is the one from regime 3 to 1, but the confidence level is only 75%. The weather regime in a sector shifted eastward from our Atlantic sector and the most robust low-frequency





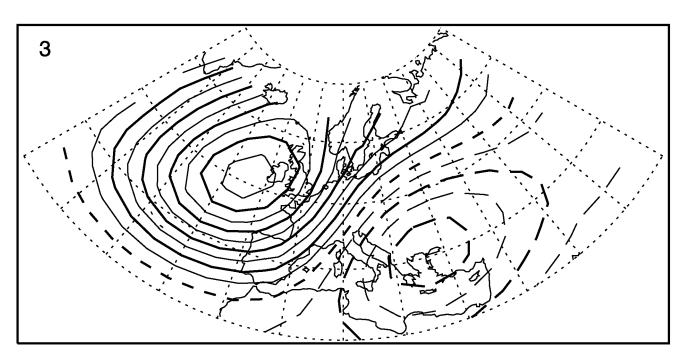


Fig. 15 The centroids of the three regimes found for the LGM case, with a sector covering $50\,^{\circ}\text{W}-70\,^{\circ}\text{E}$, $30-70\,^{\circ}\text{N}$. The variable represented is the z500 anomaly, with contours every 10 m from -200 to 200 m, zero contour *short-dashed*, negative contours *long-dashed lines*

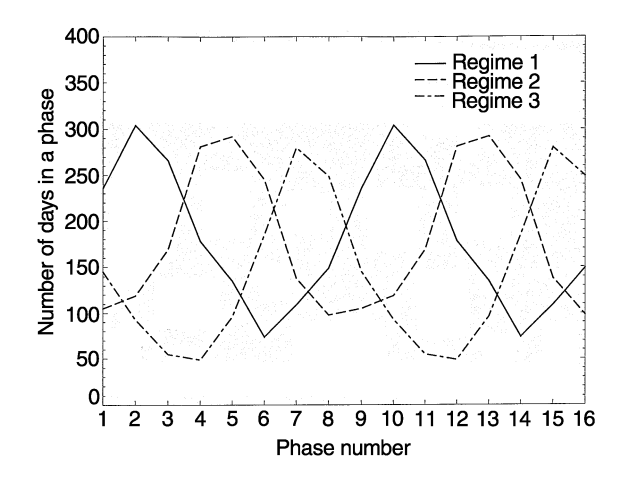


Fig. 16 Number of days of regime stays in a phase of the oscillation shown in Fig. 14, for the eight phases of the oscillation, repeated for clarity

Table 4 Number of transitions between the three regimes of Fig. 15. These transitions have been computed for episodes longer than 5 days, to retain the low-frequency variability only

То	1	2	3
From			
1	25	42	15
2	26	16	32
3	26	25	6

Table 5 Percentage of Monte-Carlo elements with a number of transitions higher than for the LGM data (matrix C from Vautard et al. 1990)

То	1	2	3
From 1 2 3	5.6% 25.6% 25.1%	0.1% 44.2% 28.5%	82.5% 6.6% 98.4%

oscillation found for this Atlantic sector are therefore clearly linked. Such connections between large-scale low-frequency oscillations and weather regimes have also been found for the present-day observations by Plaut and Vautard (1994).

5 Conclusions and perspectives

In this study, we have focused on the intraseasonal variability of the North Atlantic and European circulation in the climates of the present, the Last Glacial Maximum and the Inception of the Lst Glaciation. This variability has been mainly analyzed in terms of weather regimes. Our main goal was to investigate if those were similar for the different boundary conditions corresponding to past climates and whether climate differences could be described using the differences in the populations of the weather regimes.

We have first shown that the atmospheric general circulation model we use is capable of reproducing the observed weather regimes quite satisfactorily. We find that the characterization of climate using weather regimes is beneficial in the case of the Inception of the Last Glaciation, where the changes in regime populations are a good summary of the climate changes and reinforce the conclusions drawn from a study of the changes in the climatologies, i.e. a more northeastward position of the tail of the storm-track, favouring precipitation over northwestern Europe and in particular over the site of growth of the Fennoscandian ice-sheet: the atmosphere responds to the forcing mainly by the

increase in the population of the blocking regime and the decrease in the population of the regime which has the jet-stream most southward, the other two regimes remaining unaffected. These changes describe the differences of storminess and precipitation at ILG very well, but the changes in other variables such as the surface air temperature remain to be examined in more detail.

The study of weather regimes in the Last Glacial Maximum simulation is a clear demonstration that weather regimes, even though they are usually considered to be the product of the internal variability of the atmosphere, are sensitive to large changes in the boundary conditions. Indeed, in this case, no weather regime can be defined, and weather regimes from the CTRL experiment are irrelevant to the analysis of the climate differences. This could be inferred from the fact that the composites for this simulation on the weather regimes from the control are not similar to these regimes. In fact, the low-frequency variability over the Atlantic sector in the LGM simulation proves to be dominated by large-scale oscillations that do not have particularly persistent states. Over a sector located further eastward, the data is classifiable into three regimes that are linked to the low-frequency oscillations, therefore showing the importance of this phenomenon. Further work will concern the source of the dominant oscillation over the Atlantic domain, which has not been explored in the present work and the mechanisms of low-frequency variability and regime transitions. Also, weather regimes will be analyzed in simulations of the climates of 15000, 9000 and 6000 years ago to clarify for which boundary conditions weather regimes cease to be similar to present-day ones and to determine the role of the orographic and SST differences in the changes in weather regimes.

In a palaeoclimate perspective, our results cannot be directly validated from palaeoclimatic indicators. However, the concept of weather regimes could be important in palaeodata interpretation. One can easily imagine that some palaeoindicators are more sensitive to the variation in one regime than in the others. For example, indicators of wind (Allen 1994) are sensitive to their maximum values and hence could be more sensitive to a regime associated with very perturbed weather than a blocked regime. The present dust transport over the Atlantic and the Mediterranean has been shown to be linked to the NAO index (Moulin et al. 1997), and given the type of weather systems responsible for this transport, it would be worth investigating its dependence on intraseasonal variability. It would be all the more interesting given that dust transport is an important phenomenon in glacial times (De Angelis et al. 1987; Mayewski et al. 1994). The interpretation of palaeodata thanks to model simulations could therefore be revisited, taking into account the timescales characteristic of the palaeoindicator responses.

Acknowledgements This work has been funded by European grant ENV4-CT97-5082 (M.K.) and the PMIP simulation has been performed in the framework of the PMIP project (EC contract ENV4-CT95-0075). This is LSCE contribution number 0256.

References

- Allen JRL (1994) Palaeowind: geological criteria for direction and strength. In: Allen JR, Hoskins BJ, Sellwood BW, Spicer RA, Valdes PJ (eds) Palaeoclimates and their modelling, with special reference to the Mesozoic era, Chapman et al. pp. 27–34
- Ayrault F, Lalaurette F, Joly A Loo C (1995) North Atlantic ultra high frequency variability. Tellus 47A:671-696
- Barnola JM, Raynaud D, Korotkevich YS, Lorius C (1987) Vostok ice core provides 160 000-year record of atmospheric CO₂. Nature 329:408-414
- Berger A (1980) The Milankovitch astronomical theory of paleoclimates: a modern review. Vistas Astron 24:103–122
- Berger A, Loutre MF (1991) Insolation values for the climate of the last 10 million years. Quat Sci Rev 10:297-317
- Blackmon ML, Wallace JM, Lau NC, Mullen SJ (1977) An observational study of the northern hemisphere wintertime circulation. J Atmos Sci 34:1040–1053
- Blender R, Fraedrich K, Lunkeit F (1997) Identification of cyclonetrack regimes in the North Atlantic. QJR Meteorol Soc 123:727-741
- Carnell RE, Senior CA, Mitchell JFB (1996) An assessment of measures of storminess: simulated changes in Northern Hemisphere winter due to increasing CO₂. Clim Dyn 12:467-476
- Charney JG, De Vore JG (1979) Multiple flow equilibria in the atmosphere and blocking. J Atmos Sci 36:1205-1216
- Cheng X, Wallace JM (1993) Cluster analysis of the northern hemisphere wintertime 500-hPa height field: spatial patterns. J Atmos Sci 50:2674–2696
- CLIMAP (1981) Seasonal reconstructions of the earth's surface at the Last Glacial Maximum. Map Chart Series MC-36, Geological Society of America, Boulder, Colorado
- CLIMAP (1984) The last interglacial ocean. Quat Res 21:123–224 Cortijo E, Duplessy JC, Labeyrie L, Leclaire H, Duprat J, van Weering TCE (1994) Eemian cooling in the Norwegian Sea and North Atlantic ocean preceding continental ice-sheet growth. Nature 372:446–449
- D'Andrea F, Tibaldi S, Blackburn M, Boer G, Déqué M, Dix MR, Dugas B, Ferranti L, Iwasaki T, Kitoh A, Pope V, Randall D, Roeckner E, Straus D, Stern W, Van Den Dool H, Williamson D (1996) Northern hemisphere atmospheric blocking as simulated by 15 atmospheric general circulation models in the period 1979–1988 (results from an AMIP diagonostic subproject). Tech Rep WRCP-96; WMO/TD-No. 784, WRCP-WMO
- D'Andrea F, Tibaldi S, Blackburn M, Boer G, Déqué M, Dix MR, Dugas B, Ferranti L, Iwasaki T, Kitoh A, Pope V, Randall D, Roeckner E, Straus D, Stern W, Van Den Dool H, Williamson D (1998) Northern Hemisphere atmospheric blocking as simulated by 15 atmospheric general circulation models in the period 1979–1988. Clim Dyn 14:385–407
- De Angelis M, Barkov NI, Petrov VN (1987) Aerosol concentrations over the last climatic cycle (160 kyr) frm an Antarctic ice core. Nature 325:318-321
- Delworth TL (1996) North Atlantic interannual variability in a coupled ocean-atmosphere model. J Clim 9:2356-2375
- DeNoblet NI, Prentice IC, Joussaume S, Texier D, Botta A, Haxeltine A (1996) Possible role of atmosphere-biosphere interactions in triggering the last glaciation. Geophys Res Lett 23:3191–3194
- Dole RM (1986) Persistent anomalies of the extratropical northern hemisphere wintertime circulation: structure. Mon Weather Rev 114:178–207
- Dole RM, Gordon ND (1983) Persistent anomalies of the extratropical northern hemisphere wintertime circulation: geographi-

- cal distribution and regional persistence characteristics. Mon Weather Rev 111:1567–1586
- Dong B, Valdes PJ (1995) Sensitivity studies of northern hemisphere glaciation using an atmospheric general circulation model. J Clim 8:2471-2496
- Ducoudré NI, Laval K, Perrier A (1993) SECHIBA, a new set of parameterizations of the hydrologic exchanges at the land-atmosphere interface within the LMD Atmospheric General Circulation Model. J Clim 6:248–273
- Dzerdzeevskii B (1962) Fluctuations of climate and of general circulations of the atmosphere in extra-tropical latitudes of the Northern Hemisphere and some problems of dynamic climatology. Tellus 14:328–336
- Ferranti L, Molteni F, Brankovič Č, Palmer TN (1994a) Diagnosis of extra-tropical variability in seasonal integrations of the ECMWF model. Q J R Meteorol Soc 7:849–868
- Ferranti L, Molteni F, Palmer TN (1994b) Impact of localized tropical and extratropical SST anomalies in ensembles of seasonal GCM integrations. Q J R Meteorol Society 120:1613–1645
- Fraedrich K (1990) European grosswetter during the warm and cold extremes of the El Niño/Southern Oscillation. Int J Climatol 10:21-31
- Fraedrich K (1994) An ENSO impact on Europe? a review. Tellus 46A: 541–552
- Fraedrich K. Müller K, Kuglin R (1992) Northern Hemisphere circulation regimes during the extremes of the El Niño/Southern Oscillation. Tellus 44A:33-40
- Fraedrich K, Bantzer C, Burkhardt U (1993) Winter climate anomalies in Europe and their associated circulation at 500 hpa. Clim Dyn 8:161-175
- Gallimore RG, Kutzbach JE (1996) Role of orbitally induced changes in tundra area in the onset of glaciation. Nature 381: 503-505
- Ghil M, Childress S (1987) Topics in geophysical fluid dynamics: atmospheric dynamics, dynamo theory, and climate dynamics. Springer-Verlag, Berlin Heidelberg New York, 485 pp
- Ghil M, Mo K (1991) Intraseasonal oscillations in the global atmosphere. Part I: northern hemisphere and tropics. J Atmos Sci 48:752-779
- Guilderson TP, Fairbanks RG, Rubenstone JL (1994) Tropical temperature variations since 20 000 years ago: modulating interhemispheric climate change. Science 263:663–665
- Hall NMJ, Hoskins BJ, Valdes PJ, Senior CA (1994) Storm tracks in a high-resolution GCM with doubled carbon dioxide. Q J R Meteorol Soc 120:1209-1230
- Hall NMJ, Dong B, Valdes PJ (1996a) Atmospheric equilibrium instability and energy transport at the last glacial maximum. Clim Dyn 12:497–511
- Hall NMJ, Valdes PJ, Dong B (1996b) The maintenance of the last great ice sheets: a UGAMP GCM study. J Clim 9:1004-1019
- Harzallah A, Sadournmy R (1995) Internal versus SST-forced atmospheric variability as simulated by an atmospheric general circulation model. J Clim 8:474–495
- Hays JD, Imbrie J, Shackleton NJ (1976) Variations in the Earth's orbit: pacemaker of the ice ages. Science 194:1121-1132
- Hoskins BJ, Hsu HH, James IN, Masutani M, Sardeshmukh PD, White GH (1989) Diagnostics of the global atmospheric circulation based on ECMWF analyses 1979–1989. Tech Rep 27, WRCP
- Joussaume S, Taylor K (1995) Status of the Paleoclimate Modeling Intercomparison Project (PMIP). In: Proceedings of the first international AMIP scientific conference (Monterrey, California, USA, 15–19 May 1995), pp 425–430, WRCP-92
- Kageyama M, Valdes PJ, Ramstein G, Hewitt CD, Wyputta U (1999) Northern Hemisphere storm-tracks in present day and last glacial maximum climate simulations: a comparison of the European PMIP models. J Clim 12:742-760
- Kimoto M, Ghil M (1993) Multiple flow regimes in the northern hemisphere winter. Part II: sectorial regimes and preferred transitions. J Atmos Sci 50:2645-2673

- Kushnir Y (1987) Retrograding wintertime low-frequency disturbances over the North Pacific Ocean. J. Atmos Sci 44:2727-2742
- Kutzbach JE, Guetter PJ (1986) The influence of changing orbital parameters and surface boundary conditions on climate simulations for the past 18 000 years. J Atmos Sci 43:1726–1759
- Lau NC (1988) Variability of the observed midlatitude storm tracks in relation to low-frequency changes in the circulation pattern. J Atmos Sci 45:2718-2743
- Ledley TS, Chu S (1994) Global warming and the growth of ice sheets. Clim Dyn 9:213-219
- Manabe S, Broccoli AJ (1985) The influence of continental ice-sheets on the climate of an ice age. J Geophys Res 90:2167–2190
- Marcus SL, Ghil M, Dickey JO (1994) The extratropical 40-day oscillation in the UCLA General Circulation Model. Part I: atmospheric angular momentum. J Atmos Sci 51:—1431-1446
- Masson V, Joussaume S, Pinot S, Ramstein G (1998) Impact of parameterizations on simulated winter mid-Holocene and Last Glacial Maximum climatic changes in the Northern Hemisphere. J Geophys Res 103(D8):8935–8946
- Mayewski PA, Meeker LD, Whitlow S, Twickler MS, Morrison MC, Bloomfield P, Bond GC, Alley RB, Gow AJ, Grootes PM, Meese DA, Ram M, Taylor KC, Wumkes W (1994) Changes in atmospheric circulation and ocean ice cover over the North Atlantic during the last 41 000 years. Science 263:1747–1751
- Michelangeli PA (1996) Variabilité atmosphérique basse-fréquence observée et simulée aux latitudes tempérées. PhD Thesis, Université Pierre et Marie Curie, Paris, 190 pp
- Michelangeli PA, Vautard R, Legras B (1995) Weather regimes: recurrence and quasi stationarity. J. Atmos Sci 52:1237-1256
- Miller GH, de Vernal A (1992) Will greenhouse warming lead to Northern Hemisphere ice-sheet growth? Nature 355:244–246
- Mo K, Ghil M 1(988) Cluster analysis of multiple planetary flow regimes. J Geophys Res 93(D9):10927-10952
- Molteni F, Tibaldi S, Palmer TN (1990) Regimes in the wintertime circulation over the northern extratropics. I: observational evidence. Q J R Meteorol Soc 116:31-67
- Molteni F, Ferranti L, Palmer TN, Viterbo P (1993) A dynamical interpretation of the global response of Equtorial Pacific SST anomalies. J Clim 6:777-795
- Moulin C, Lambert CE, Dulac F, Dayan U (1997) Control of atmospheric export of dust from North Africa by the North Atlantic Oscillation. Nature 387:691-694
- Nakamura H, Wallace JM (1990) Observed changes in baroclinic wave activity during the life cycles of low-frequency circulation anomalies. J Atmos Sci 47:1100–1116
- Palmer TN (1993) A nonlinear perspective on climate change. Weather 48:314–326
- Palmer TN (1998) Nonlinear dynamics and climate change: Rossby's legacy. Bull Am Meteorol Soc 79:1411–1423
- Peltier WR (1994) Ice age paleotopography. Science 265:195–201
- Plaut G, Vautard R (1994) Spells of low-frequency oscillations and weather regimes in the northern hemisphere. J. Atmos Sci 51:210-236
- Ponater M, König W, Sausen R, Sielmann F (1994) Circulation regime fluctuations and their effect on intraseasonal variability in the ECHAM climate model. Tellus 46A:265–285
- Ramstein G, Fabre A, Pinto S, Ritz C, Joussaume S (1997) Ice-sheet mass balance during the Last Glacial Maximum. Ann Glaciol 25:145-152

- Raynaud D, Jouzel J, Barnola JM, Chappellaz J, Delmas RJ, Lorius C (1993) The ice record of greenhouse gases. Science 259: 926–934
- Rex DF (1950a) Blocking action in the middle troposphere and its effect upon regional climate. I. An aerological study of blocking action. Tellus 2:196–211
- Rex DF (1950b) Blocking action in the middle troposphere and its effect upon regional climate. II. The climatology of blocking action. Tellus 2:275–301
- Rind D (1987) Components of the ice age circulation. J Geophys Res 92:4241–4281
- Rind D, Peteet D (1985) Terrestrial conditions at the Last Glacial Maximum and CLIMAP sea-surface temperature estimates: are they consistent? Quat Res 24:1-22
- Robertson AW, Ghil M, Latif M (1999) Interdecadal changes in atmospheric low-frequency variability with and without boundary forcing. J Atmos Sci in press
- Royer JF, Déqué M, Pestiaux P (1983) Orbital forcing of the inception of the laurentide ice sheet? Nature 304:43–46
- Ruddiman WF, McIntyre A (1979) Warmth of the subpolar North Atlantic ocean during Northern Hemisphere ice-sheet growth. Science 204:173-175
- Sadourny R, Laval K (1984) January and July performance of the LMD general circulation model. In: Berger A, Nicolis C (eds) New Perspectives in Climate Modelling, vol 16 of Developments in Atmospheric Science, Elsevier, Amsterdam pp 173–198
- Schmith T, Kaas E, Li TS (1998) Northeast Atlantic winter storminess 1875–1995 re-analysed. Clim Dyn 14: 529–536
- Seluchi M, Serafini YV, Le Treut H (1998) The impact of the Andes on transient atmospheric systems: a comparison between observations and GCM results. Mon Weather Rev 126:895-912
- Syktus J, Gordon H, Chappell J (1994) Sensitivity of a coupled atmosphere-dynamic upper ocean GCM to variations of CO₂, solar constant, and orbital forcing. Geophys Res Lett 21:1599-1602
- Texier D, De Noblet N, Harrison SP, Haxeltine A, Jolly D, Joussaume S, Laarif F, Prentice IC, Tarasov P (1997) Quantifying the role of biosphere-atmosphere feedbacks in climate change: coupled model simulations for 6000 years BP and comparison with paleodata for northern Eurasia and northern Africa. Clim Dyn 13:865-882
- Tibaldi S, D'Andrea F, Tosi E, Roeckner E (1997) Climatology of Northern Hemisphere blocking in the ECHAM model. Clim Dyn 13:649-666
- Vautard R (1990) Multiple weather regimes over the North Atlantic: analysis of precursors and successors. Mon Weather Rev 118:2056–2081
- Vautard R, Legras B (1988) On the source of midlatitude low-frequency variability. Part II: equilibration of weather regimes. J Atmos Sci 45:2845–2867
- Vautard R, Mo KC, Ghil M (1990) Statistical significance test for transition matrices of atmospheric Markov chains. J Atmos Sci 47:1926–1931
- Wallace JM, Gutzler DS (1981) Teleconnections in the geopotential height field during the Northern Hemisphere winter. Mon Weather Rev 109:784–812
- Wallace JM, Smith C, Jiang Q (1990) Spatial patterns of atmosphere-ocean interactions in the northern winter. J Clim 3:990-998